Reparative macrophages regulate fibrosis by attenuating apoptosis and senescence of fibroblasts

Manabu Shiraishi[1,2], Atsushi Yamaguchi[1] and Ken Suzuki[2]

[1]Department of Cardiovascular Surgery, Saitama Medical Center, Jichi Medical University, Saitama 330-0834, Japan.

[2]William Harvey Research Institute, Barts and The London School of Medicine and Dentistry, Queen Mary University of London, London EC1M 6BQ, United Kingdom.

Address correspondence to:

Manabu Shiraishi, Department of Cardiovascular Surgery, Saitama Medical Center, Jichi Medical University, Saitama 330-0834, Japan,.

Tel: +81-48-647-2111; E-mail: manabu@omiya.jichi.ac.jp

Character count: 11797

Abstract

Appropriate fibrotic tissue formation after myocardial infarction (MI) is crucial to maintain the heart structure. Reparative or M2-like macrophages play a vital role in fibrosis by activating cardiac fibroblasts after MI. This study investigated the molecular and cellular mechanisms through which post-MI fibrosis is formed by focusing on the role of the M2-like macrophage subset and examined how to control fibrosis formation. We found that cardiac fibroblasts in the infarcted mouse heart showed apoptosis and senescence, both of which are associated with the fibrotic process. Moreover, some of the molecular mechanism underlying fibrotic tissue formation in the infarcted myocardium was attenuation of apoptosis and senescence of fibroblasts by M2-like macrophage-derived neuregulin 1 (Nrg1)/epidermal growth factor receptor (ErbB) signaling. *In vitro* and *in vivo* experiments showed that selective Nrg1 receptor inhibition exacerbated senescence of cardiac fibroblasts, which resulted in excessive progression of fibrosis. These results highlight previously unidentified anti-apoptotic and anti-senescence effects of the Nrg1/ErbB signaling system on cardiac fibroblasts after MI.

Key words:

apoptosis / fibroblast / fibrosis / macrophage / myocardial infarction / senescence

Introduction

Myocardial infarction (MI) is a leading cause of mortality and disability. Even survivors of acute MI frequently develop heart failure because of adverse ventricular remodeling (Dickstein, Cohen-Solal et al., 2008, Zhu, Li et al., 2013). Because the human heart has an insufficient regenerative ability, connective tissue formation is essential to maintain integrity and rigidity of the heart. However, the mechanism by which cardiac fibrosis is regulated post-MI is not fully understood.

MI causes permanent loss of hundreds of millions of cardiomyocytes (Gemberling, Karra et al., 2015). Studies have shown that even non-cardiomyocytes, including fibroblasts, disappear in large quantities through apoptosis in the infarcted area and that senescence-associated defects occur in cardiac repair post-MI (Gould, Taffet et al., 2002, Takemura, Ohno et al., 1998). Apoptosis plays an important role in the disappearance of infiltrated immune cells and interstitial cardiac cells after MI (Takemura et al., 1998). Because senescence and apoptosis of both cardiomyocytes and fibroblasts are deeply involved in the pathophysiology of left ventricular adverse remodeling and cardiac rupture after MI (Shih, Lee et al., 2011), determining the molecular mechanisms through which senescence and apoptosis are regulated during the tissue repair process after MI is important. Senescence and apoptosis are processes of growth arrest in response to cellular stress and damage, and they limit proliferation of mammalian cells (Munoz-Espin & Serrano, 2014, Sharpless & Sherr, 2015). Senescent cells show a complex phenotype characterized by cell cycle arrest mediated through p16 and p53/p21 pathways, and a unique secretory phenotype known as the senescence-associated secretory phenotype (SASP) (Coppe, Desprez et al., 2010). Cell cycle arrest plays a central role in the senescent phenotype of adult cardiomyocytes and induction of cell cycle reentry of adult cardiomyocytes promotes cardiac repair post-MI (Alam, Haile et al., 2019). Anti-apoptotic substances and Fas receptor competitive inhibitors suppress cardiomyocyte apoptosis, which decrease the infarct size and improve cardiac functions after MI (Hayakawa, Takemura et al., 2003). Previous studies have shown that even non-cardiomyocytes, including fibroblasts, undergo apoptosis in the infarcted area (Gould et al., 2002, Takemura et al., 1998). Therefore, senescence and/or apoptosis of cardiac fibroblasts may be involved in the tissue repair process after MI. A recent study found that senescent

cardiac fibroblasts, in which expression of major senescence regulator p53 was significantly upregulated, had markedly accumulated in the heart after MI, p53-mediated fibroblast senescence limited cardiac collagen production, and inhibition of p53 increased reparative fibrosis. Knockdown of endogenous p53 by small interfering RNA and increased expression of p53 protein by adenoviral transduction are useful methods to investigate the specific contribution of p53-mediated cardiac collagen production to the post-MI heart (Zhu et al., 2013). However, these methods have limited capabilities to identify the cellular and molecular mechanisms by which a particular subset of immune cells is responsible for regulation of fibroblast senescence and collagen production. To some extent, senescence of fibroblasts restricts fibrosis, but the long-term presence of this condition is deleterious to the tissue repair process (Childs, Li et al., 2018). Proper fibrosis after MI is crucial to maintain the heart structure, but excessive fibrosis eventually leads to heart failure. Therefore, adjusting the balance between profibrotic and anti-fibrotic environments is important for a successful regenerative outcome. To understand the tissue repair process of fibrosis, it is necessary to clarify intercellular communication between senescent and apoptotic fibroblasts and surrounding cells.

Recent studies have shown that macrophages are essential for regeneration of the neonatal mouse heart (Aurora, Porrello et al., 2014). We have previously shown that reparative or M2-like macrophages play a pivotal role in fibrotic tissue formation post-MI through promotion of proliferation and activation of cardiac fibroblasts (Shiraishi, Shintani et al., 2016). However, the molecular mechanism used by M2-like macrophages in the anti-senescence and anti-fibrotic environment after MI remains unknown. We hypothesized that M2-like macrophages play a vital role in attenuating apoptosis and senescence that cause excessive fibrosis of cardiac fibroblasts.

Neuregulin 1 (Nrg1) is one of the neuregulin genes (*Nrg1–Nrg4*) that belong to the epidermal growth factor family (Fuller, Sivarajah et al., 2008, Meyer, Yamaai et al., 1997) and Nrg1/epidermal growth factor receptor (ErbB) signaling systems play essential roles in protection and proliferation of cardiomyocytes in response to injury (Bersell, Arab et al., 2009, Hedhli, Huang et al., 2011, Lemmens, Doggen et al., 2007, Polizzotti, Ganapathy et al., 2015, Yutzey, 2015). Although the association between Nrg1 and protection of cardiomyocytes has been studied for several decades (Bersell et al., 2009, Hedhli et al., 2011, Lemmens et al., 2007, Polizzotti et al., 2015, Yutzey, 2015), the roles of

Nrg1 in protecting cardiac fibroblasts and post-MI regeneration have not been fully established. A recent study has shown that Nrg1 enhanced cellular proliferation and viability, which was linked to Nrg1/ErbB4 signaling activity, in normal human cardiac ventricular fibroblasts (Kirabo, Ryzhov et al., 2017). However, under *in vivo* post-MI conditions, the relationship between M2-like macrophage-derived Nrg1/ErbB4 signaling activity and anti-senescence and anti-apoptotic effects in cardiac fibroblasts have not been identified. Another study has indicated that Nrg1 exerted anti-fibrotic effects in a mouse model of angiotensin II-induced myocardial hypertrophy, which were explained by the anti-fibrotic effect of Nrg1 linked to the anti-inflammatory activity Nrg1/ErbB4 signaling in macrophages (Vermeulen, Hervent et al., 2017). Furthermore, Nrg1-loaded poly-microparticles were used in a previous study to induce macrophage polarization toward an anti-inflammatory phenotype, which prevented macrophages from transitioning toward the inflammatory phenotype and enhanced cardiac repair after MI (Pascual-Gil, Abizanda et al., 2019). These studies investigated the contribution of Nrg1/ErbB4 signaling in macrophages and macrophage polarization toward an anti-inflammatory phenotype to assist cardiac tissue repair, but the significance of Nrg1/ErbB4 signaling activity in cardiac fibroblasts for anti-fibrotic effects has not been clarified. Therefore, it is important to accumulate more convincing evidence to determine the precise roles of M2-like macrophage-derived Nrg1 after MI in senescence, apoptosis, and the fibrotic phenotype of fibroblasts using a more appropriate model, which will also facilitate dissecting the underlying mechanism. Therefore, this study investigated the molecular and cellular mechanism by which post-MI fibrosis is formed with a focus on the role of the M2-like macrophage subset and examined how to control fibrosis formation. Our findings may help to clarify the pathophysiology of fibrosis after MI and form the basis for development of new therapeutic methods focused on senescence and apoptosis of cardiac fibroblasts.

Results

Cardiac fibroblasts undergo apoptosis and senescence after MI

126 We investigated cellular senescence and apoptosis in post-MI fibrosis of an MI mouse model
127 established coronary artery ligation. Obvious fibrotic tissue formation and increased myocardial
128 expression of fibrosis-associated genes (i.e., alpha-smooth muscle actin [*αSMA*], *Col1a1*, and *Col3a1*)
129 were observed in the infarct area as early as day 7 post-MI (Fig EV1A and B). This change was
130 associated with an increase in thymocyte antigen 1 $(Thy1)^+$ fibroblasts and $Thy1^+\alpha SMA^+$
131 myofibroblasts in the infarct area (Fig EV1C and D) with a peak at day 7 post-MI. Approximately
132 40% and 15% of $Thy1^+$ fibroblasts were positive for cleaved caspase 3 in the infarct area on days 7
133 and 28 after MI, respectively, which suggested robust apoptosis of cardiac fibroblasts. Cleaved
134 caspase 3-positive cardiac fibroblasts were rarely found in the non-infarcted remote area (Fig 1A).
135 Simultaneously, senescence-associated β-galactosidase (SA-β-gal)-positive cells were found in the
136 same infarct area. These cells showed a spindle shape with many cytoplasmic processes, which
137 suggested that they were fibroblasts (Fig 1B). Additionally, myocardial expression of
138 senescence-associated genes (i.e., *SA-β-gal*, *p16*, *p53*, and *p21*) (Krizhanovsky, Yon et al., 2008,
139 Munoz-Espin & Serrano, 2014, Sharpless & Sherr, 2015, van Deursen, 2014, Zhu et al., 2013) was
140 upregulated in the infarct area compared with the non-infarcted remote area (Fig 1C). Increased
141 apoptosis and senescence of fibroblasts and other types of cardiac cells had exacerbated myocardial
142 inflammation post-MI (Fig EV1E). Taken together, these results suggest that apoptosis and
143 senescence occur in cardiac fibroblasts during fibrotic tissue formation in the post-MI heart.
144
145 ***Nrg1 is upregulated in the infarcted myocardium, while cardiac fibroblasts express Nrg1 receptors***
146 Quantitative reverse transcription-polymerase chain reaction (qRT-PCR) showed that *Nrg1* was
147 upregulated in the infarct area of the mouse heart with a peak on day 7 post-MI (Fig 2A).
148 Immunohistochemistry (IHC) showed that most $Thy1^+$ cardiac fibroblasts that had accumulated in
149 infarcted and remote areas were stimulated to express ErbB2 and ErbB4 that are coreceptors of Nrg1
150 (Lemmens et al., 2007, Olayioye, Neve et al., 2000, Uray, Connelly et al., 2002) (Fig 2B). These
151 results suggest that Nrg1 is involved in the proliferation and viability of cardiac fibroblasts after MI.
152
153 ***M2-like macrophages accumulate in the infarct area and express Nrg1***

M2-like macrophages play a major role in fibrotic tissue formation post-MI (Shiraishi et al., 2016). IHC showed that $CD206^+$ M2-like macrophages had accumulated in the infarct area with a peak at day 7 post-MI (Fig 3A). We found that the left ventricular myocardium of adult mice contained $CD11b^+F4/80^+$ macrophages, more than 90% of which were positive for CD206. Conversely, the majority of $CD206^+$ cardiac cells were positive for both F4/80 and CD11b in both normal and post-MI hearts in our previous study (Shiraishi et al., 2016). We further confirmed that $CD206^+$ cells were also positive for F4/80 in intact and MI hearts (Fig 3B). Interestingly, this change in M2-like macrophages post-MI corresponded to a change in the occurrence of cardiac fibroblasts post-MI (Fig EV1C). Microarray analysis showed that $CD206^+F4/80^+CD11b^+$ M2-like macrophages collected from hearts on day 7 after MI had a different molecular signature than those from intact hearts (Fig EV2A). A range of anti-inflammatory and reparative genes were upregulated in $CD206^+F4/80^+CD11b^+$ M2-like macrophages from MI hearts compared with intact hearts (Supplemental Figure 2B; full data are available in the Gene Expression Omnibus [GEO] database; GSE69879). Importantly, gene ontology analysis showed that M2-like macrophages collected from hearts on day 7 after MI were associated with regulation of apoptosis and cell death (Fig EV2C). Considering the differences in gene expression of cardiac $CD206^+F4/80^+CD11b^+$ M2-like macrophages before and after MI, we focused on the increased *Nrg1* expression level in $CD206^+F4/80^+CD11b^+$ cardiac M2-like macrophages after MI (Fig 3C), which was confirmed by qRT-PCR and IHC (Fig 3D and E). By searching for genes related to proliferation and viability in the genetic information obtained from HomoloGene (https://www.ncbi.nlm.nih.gov/homologene), we hypothesized that Nrg1 might be a critical mediator of anti-senescence and anti-apoptosis activation in cardiac fibroblasts. These data suggest that cardiac M2-like macrophages are a source of upregulated Nrg1 post-MI.

Bone marrow-derived macrophages attenuate H_2O_2-induced apoptosis and senescence of cardiac fibroblasts via Nrg1 secretion

We next investigated the role of macrophages in regulating senescence and apoptosis in *in vitro* coculture of cardiac fibroblasts with bone marrow-derived macrophages (BMDMs) using a Boyden Chamber system in which cells were able to be independently stained or genetically analyzed without

mixing with each other (Shiraishi et al., 2016, Suzuki, Arumugam et al., 2014) (Fig EV3A). H_2O_2 was used to induce apoptosis and senescence of fibroblasts (Fig EV3B and C). BMDMs cultured in the presence of H_2O_2 showed an M2-like macrophage phenotype (Fig EV4A and B). Similar to *in vivo* findings after MI (Figs 2B, 3D and E), we observed increased expression of *Nrg1* in BMDMs and *ErbB2* and *ErbB4* in H_2O_2-treated cardiac fibroblasts (Fig EV5A–C). Such gene expression was upregulated in response to H_2O_2. Phase-contrast microscopy showed that fibroblasts treated with H_2O_2 had an enlarged, flattened, senescent morphology, which became a spindle-shaped healthy form after coculture with BMDMs. Senescent fibroblasts treated with an anti-ErbB4 antibody (Ab), which is a competitive inhibitor of Nrg1, displayed the same gross morphology as senescent fibroblasts treated with H_2O_2. Recombinant Nrg1 similarly returned the gross morphology of senescent fibroblasts treated with H_2O_2 to a spindle-shaped healthy form (Fig 4A). SA-β-gal staining showed that approximately 20% of fibroblasts treated with H_2O_2 became positive for SA-β-gal. This change was significantly attenuated by coculture with BMDMs, whereas addition of the anti-ErbB Ab eliminated this anti-senescence effect of BMDMs. Furthermore, administration of recombinant Nrg1 suppressed H_2O_2-induced senescence of fibroblasts (Fig 4B). The ratio of cleaved caspase 3^+ apoptotic cells among cardiac fibroblasts was also significantly increased by H_2O_2 stimulation (Fig 4C). Coculture with BMDMs markedly attenuated this apoptotic change in fibroblasts. The anti-apoptotic effect of BMDMs was attenuated by addition of the anti-ErbB Ab, whereas administration of recombinant Nrg1 suppressed H_2O_2-induced apoptosis of fibroblasts. Immunolabeling of Ki67 showed that the proliferative property of cardiac fibroblasts was significantly attenuated by H_2O_2 stimulation (Fig 4D). Coculture with BMDMs markedly improved these cellular activities in fibroblasts. The effects of BMDMs were attenuated by addition of the anti-ErbB Ab, whereas administration of recombinant Nrg1 suppressed H_2O_2-induced functional deterioration of fibroblasts. H_2O_2 stimulation reduced the proliferative activity of cardiac fibroblasts, which was rescued by coculture with BMDMs. This effect of BMDMs was eliminated by addition of the anti-ErbB Ab. Recombinant Nrg1 administration showed a strong ability to increase proliferation of fibroblasts. These results collectively suggest that M2-like macrophages reduce apoptosis and senescence of fibroblasts through secretion of Nrg1.

BMDMs promote activation of fibroblasts and collagen synthesis

Immunocytological staining showed that, although independent H_2O_2 treatment did not affect conversion of cardiac fibroblasts into αSMA$^+$ myofibroblasts, coculture with BMDMs and H_2O_2 stimulation activated fibroblasts. Furthermore, addition of the anti-ErbB Ab enhanced this BMDM-induced activation of fibroblasts. Moreover, addition of recombinant Nrg1 did not affect conversion of cardiac fibroblasts (Fig 5A). Changes in synthesis of types I and III collagen in fibroblasts in response to H_2O_2, BMDMs, and Nrg1 were associated with that of αSMA expression (Fig 5B and C). These results suggest that BMDMs, which have an M2-like phenotype (Fig EV4A and B), induce activation of fibroblasts to convert into myofibroblasts and this activation is accelerated with progression of fibroblast senescence. Osteopontin (*Spp1*) is a major mediator of M2-like macrophage-induced cardiac fibroblast activation (Shiraishi et al., 2016). *Spp1* expression was increased in BMDMs in response to H_2O_2 (Fig EV6A). Conversely, other profibrotic factors, including *Tgfb1* and *Pdgfa* (Shinde & Frangogiannis, 2014, van den Borne, Diez et al., 2010), were not upregulated in M2-like macrophages (Fig EV6B).

Phosphatidylinositol 3-kinase/protein kinase B signaling is associated with BMDM-attenuated apoptosis and senescence of cardiac fibroblasts through Nrg1

We next investigated the potential mechanism underlying attenuation of apoptosis of cardiac fibroblasts and senescence by BMDM-derived Nrg1. The phosphatidylinositol 3-kinase (PI3K)/protein kinase B (Akt) signaling pathway is downstream of the ErbB pathway. Western blot analysis showed that coculture with BMDMs increased PI3K/Akt activation in fibroblasts, but this was attenuated by addition of the anti-ErbB Ab. Recombinant Nrg1 administration also activated the PI3K/Akt pathway in fibroblasts (Fig 6A). To determine the possible relationship between senescence-associated p16/p53/p21 and Nrg1/ErbB/PI3K/Akt signaling pathways, we examined mRNA expression levels of senescence-associated genes (*p53*, *p21*, *p16*, and *SA-β-gal)* (Fig 6B), cell cycle-associated genes (cyclin-dependent kinase 4 [*Cdk4*], cyclin-dependent kinase 6 [*Cdk6*],

cyclin-dependent kinase 2 [*Cdk2*], and *Ki-67*) (Fig 6C), a p53 suppressor gene (murine double minute 2 [*MDM2*]) (Fig 6D), a cell survival-associated gene (mechanistic target of rapamycin [*mTOR*]) (Fig 6E), and SASP-associated gene (interleukin-6 [*IL-6*]) (Fig 6F). Expression of senescence-associated genes (*p16* and *p21*) and an SASP-associated gene (*IL-6*) was significantly higher and expression of cell cycle-associated genes (*Cdk4*, *Cdk6*, *Cdk2*, and *Ki-67*) and a cell survival-associated gene (*mTOR*) was markedly lower in fibroblasts treated with H_2O_2 compared with controls. Importantly, these changes in gene expression, including progression of senescence and inflammation, and suppression of the cell cycle recovered to those of controls after coculture with BMDMs. Addition of the anti-ErbB Ab resulted in gene expression similar to that induced by H_2O_2 treatment. Moreover, expression of senescence-associated genes (*p53*, *p16*, and *p21)* was significantly suppressed and expression of cell cycle-associated genes (*Cdk4*, *Cdk6*, *Cdk2*, and *Ki-67*) was enhanced by recombinant Nrg1 in fibroblasts treated with H_2O_2. In terms of other related genes, BMDMs enhanced expression of the p53 suppressor gene *MDM2*. These results suggest that the Nrg1/ErbB system operates downstream of PI3K/Akt signaling activation and exerts a suppressive effect on cell cycle arrest, senescence, and apoptosis. Simultaneously, this signaling activity is likely to increase cellular proliferation and survival (Fig 6G).

In vivo inhibition of Nrg1 signaling exacerbates fibrosis

We used trastuzumab to clarify the role of Nrg1 in suppressing senescence and apoptosis of cardiac fibroblasts post-MI *in vivo*. Trastuzumab is an anti-human epidermal growth factor receptor type 2 (HER2) monoclonal antibody that binds to the extracellular juxtamembrane domain of HER2. Trastuzumab is an effective treatment for HER2/neu$^+$ tumors in animals and humans (ElZarrad, Mukhopadhyay et al., 2013, Park, Jiang et al., 2010). We hypothesized that trastuzumab administration would eliminate the anti-apoptotic and anti-senescence effects of Nrg1 and therefore increase the number of senescent cardiac fibroblasts. On the basis of the *in vitro* coculture model, we also hypothesized that trastuzumab administration would encourage the progression of senescence and apoptosis of cardiac fibroblasts, which increase fibrotic scar formation in the infarcted

myocardium. We found that intraperitoneal trastuzumab injections did not affect mRNA expression in the intact heart (Fig EV7A–D).

Mice underwent surgery to induce MI and received intraperitoneal injections of either trastuzumab or vehicle only (Fig EV8A). Trastuzumab did not affect post-MI mortality or body weight (Fig EV8B and C). Gene expression profiles in the infarcted myocardium suggested that senescence and apoptosis were augmented by trastuzumab administration in the infarct area (Fig 7A–C). These changes in gene expression corresponded to an increase in apoptotic fibroblasts and senescent cardiac cells in the infarct area (Fig 7D and E). Additionally, trastuzumab administration increased fibrotic tissue formation in the infarct area (Fig 8A). In fact, Thy-1^+ fibroblasts were increased in this area (Fig 8B). The number of αSMA^+Thy1^+ myofibroblasts was also increased in association with upregulation of *αSMA*, *Col1a1*, and *Col3a*1 in the infarcted myocardium (Fig 8B and C). Increased inflammation (Fig 9A) and increased M2-like macrophages in this area (Fig 9B) may explain these findings. Trastuzumab administration might have increased senescence and apoptosis of fibroblasts and other types of cardiac cells, which exacerbated myocardial inflammation post-MI. This led to accumulation of M2-like macrophages. Such augmented inflammatory signals or an increase in the number of M2-like macrophages could accelerate proliferation of cardiac fibroblasts, while increased M2-like macrophages could promote activation of fibroblasts to convert into myofibroblasts. Subsequently, trastuzumab administration might have exacerbated fibrotic tissue formation. Interestingly, trastuzumab administration induced apoptosis- and senescence-associated gene expression in the remote area (Fig EV9A–E) in which direct ischemic damage hardly occurred post-MI. This corresponded to increased inflammation (Fig EV11A). These changes augmented the accumulation of M2-like macrophages and cardiac fibroblasts in the remote myocardium (Figs EV10B and 11A). Conversion of fibroblasts into myofibroblasts and fibrosis-associated gene expression were also induced (Fig EV12A and B). Consequently, fibrosis occurred even in the remote area (Fig EV12). These results suggest that trastuzumab augments apoptosis and senescence of cardiac fibroblasts post-MI, which results in excessive fibrosis, even in the non-infarcted remote area.

Discussion

Despite the enormous clinical importance of cellular and molecular processes underlying the formation of post-MI fibrosis, they are not well understood. To precisely determine the roles of cardiac M2-like macrophages in apoptosis and senescence of fibroblasts, we analyzed an *in vitro* experimental model in which H_2O_2-induced senescent cardiac fibroblasts were cocultured with BMDMs. This *in vitro* model reflects the *in vivo* conditions of post-MI because senescent cells attract macrophages under pathological conditions (Sasaki, Miyakoshi et al., 2010). The model allowed us to determine the precise interaction between M2-like macrophages and senescent cardiac fibroblasts. Briefly, the possible mechanism is that activation of the macrophage-derived Nrg1/ErbB/PI3K/Akt signaling pathway suppresses senescence and apoptosis of injured cardiac fibroblasts, which inhibits excessive collagen synthesis. ErbB is also expressed on the surface of macrophages and myeloid-specific ErbB gene deletion exacerbates myocardial fibrosis (Vermeulen et al., 2017). Furthermore, Nrg1-induced macrophage polarization from an inflammatory phenotype toward an anti-inflammatory phenotype enhances cardiac repair after MI (Pascual-Gil et al., 2019). Therefore, a concern might be the possibility that ErbB signaling in BMDMs was simultaneously affected when the anti-ErbB Ab was added to the culture medium in our coculture experiments. Our depletion method using the anti-ErbB Ab has limited specificity for cardiac fibroblasts. This method depletes Nrg1/ErbB signaling in both fibroblasts and BMDMs. Thus, exacerbated phenotypic changes in senescence and apoptosis were not caused by specific inhibition of Nrg1/ErbB signaling in fibroblasts. However, in the H_2O_2+Nrg1 group, only recombinant Nrg1 was added to the medium. Therefore, this group excluded the effects of Nrg1/ErbB signaling suppression in BMDMs by the anti-ErbB Ab and the results of senescence, the apoptotic phenotype, and gene expression were similar to the H_2O_2+BMDM group (Figs 4A–C and 6A, B). Therefore, our data suggested that Nrg1/ErbB signaling activity in fibroblasts had a greater effect on anti-senescence and anti-apoptotic effects in fibroblasts compared with Nrg1/ErbB signaling activity related to anti-inflammation in macrophages.

Nrg1 is a cytokine that belongs to a family of proteins structurally related to epidermal growth factor and plays essential roles in protection and proliferation of cardiomyocytes in response to injury (Bersell et al., 2009, Hedhli et al., 2011, Lemmens et al., 2007, Polizzotti et al., 2015, Yutzey, 2015).

Nrg1 is synthesized in endothelial cells near cardiomyocytes (Lemmens et al., 2007). We observed that *Nrg1* was expressed in M2-like macrophages and that it had a specific function to rescue post-MI-induced senescent and apoptotic cardiac fibroblasts. Cardiac fibroblasts expressed ErbB2/ErbB4 in the damaged myocardium on days 7 and 28 post-MI. Nrg1 binds to the ErbB4 receptor. After heterodimerization with phosphorylated ErbB2, signaling pathways that are activated downstream of ErbB2/ErbB4 signals link to the Ras-mitogen-activated protein kinase pathway and PI3K/Akt pathways (Lemmens et al., 2007). The hypertrophic response to Nrg1 is mainly dependent on Ras, whereas the anti-apoptotic and cell proliferation effects are likely to be dependent on Akt (Baliga, Pimental et al., 1999, Gelb & Tartaglia, 2011, Kuramochi, Cote et al., 2004). Therefore, Nrg1 may attenuate expression of senescence-associated genes *p53*, *p21*, and *p16* through PI3K/Akt pathways. In our study, we observed a transient increase in *p53*, *p21*, and *p16* expression in the infarcted myocardium and cultured fibroblasts. Zhu *et al*. reported that MI promotes accumulation of senescent cardiac fibroblasts in the heart and *p53* expression (Zhu et al., 2013). Increased p53 activity in response to diverse pathological stresses, such as MI, induces apoptosis (Long, Boluyt et al., 1997, Polyak, Xia et al., 1997). Stress-induced *p53* expression increases *p21* expression in response to DNA damage and induces reversible proliferative arrest that provides time for DNA repair and facilitates survival of cells (Deng, Zhang et al., 1995, Wang, Elson et al., 1997). Previous studies have shown that p21 binds to and inhibits CDK2-mediated inactivation of retinoblastoma, which subsequently prevents entry into the S phase of the cell cycle (Childs, Durik et al., 2015, Munoz-Espin & Serrano, 2014). Furthermore, p21 is important to initiate senescence in some settings, but its expression does not persist in senescent cells (Alcorta, Xiong et al., 1996, Stein, Drullinger et al., 1999). Simultaneously, increased *p16* expression is found in infarcted tissue. Irreversible proliferative arrest can be induced by p16 that inhibits two cycle-dependent kinases, CDK4 and CDK6 (Munoz-Espin & Serrano, 2014, Serrano, Lin et al., 1997). Therefore, a change in expression of these genes (i.e., *p53*, *p21*, and *p16*) in cardiac cells *in vivo* and cardiac fibroblasts *in vitro* suggests that Nrg1 is a crucial factor that controls reversible and irreversible senescence of cardiac cells after MI.

Previous reports have shown that trastuzumab efficiently stops or slows the growth of $ErbB2^+$ cells *in vitro* and inhibits the ability of cells to repair damaged DNA (ElZarrad et al., 2013, Park et al.,

2010). Our study showed that trastuzumab injection further increased senescence and apoptosis in the infarcted myocardium. As inflammation worsens, M2-like macrophages from bone marrow accumulate at the site of damaged tissue (Ikeda, Asano et al., 2018). In our study, progression of senescence and apoptosis in cardiac fibroblasts and exacerbation of inflammation induced by trastuzumab increased the accumulation of M2-like macrophages, which promoted activation of fibroblasts and excessive fibrosis. These results are consistent with our previous report indicating that interleukin 4-mediated M2-like macrophage activation induces conversion of fibroblasts into myofibroblasts for progression of fibrosis (Shiraishi et al., 2016). Osteopontin is a major mediator of M2-like macrophage-induced activation of cardiac fibroblasts (Shiraishi et al., 2016). Although we analyzed mRNA gene expression in tissue sections of the heart and not in single cells, increased expression levels of senescence-associated genes were considered to reflect senescence of fibroblasts to a certain extent. These results corresponded to *in vitro* observations using the anti-ErbB Ab. Addition of the anti-ErbB Ab further increased senescence and apoptosis. This exacerbation of senescence and apoptosis induced by the anti-ErbB Ab promoted activation of fibroblasts cocultured with BMDMs, which augmented collagen synthesis.

Interestingly, senescence and SASP-associated gene expression peaked slightly later in the remote area than in the infarct area. One possible pathological mechanism of the non-infarcted remote area is assumed to be indirect damage via SASP rather than direct cytotoxicity due to ischemia. Senescent cells autonomously induce senescence-like gene expression in their surrounding non-senescent cells through SASP (Acosta, Banito et al., 2013). Increased SASP in the infarct area might not simply affect senescence and apoptosis of cells in the infarct area, but also have a harmful influence on non-senescent cells in the remote area. All of these data suggest that trastuzumab-induced exacerbation of fibrosis is mainly mediated by progression of senescence and apoptosis in cardiac fibroblasts.

Nrg1 has been repeatedly reported to play important roles in injured cardiomyocytes (Bersell et al., 2009, Hedhli et al., 2011, Lemmens et al., 2007, Polizzotti et al., 2015, Yutzey, 2015). Injecting Nrg1 in adult mice induces cardiomyocyte cell-cycle activity and promotes myocardial regeneration, leading to improved function after myocardial infarction (Bersell et al., 2009). Nrg1 significantly

decreases apoptosis of adult cardiomyocytes under hypoxia-reoxygenation conditions (Hedhli et al., 2011). Nrg1 also has Akt-dependent anti-apoptotic effects on cardiomyocyte growth and survival (Lemmens et al., 2007). Administration of recombinant Nrg1 improves myocardial functions and reduces the prevalence of transmural scars after MI (Polizzotti et al., 2015). However, its role in cardiac fibroblasts in this context has not been well studied. Our data provide new biological insights into the molecular mechanisms by which M2-like macrophages regulate post-MI tissue repair by affecting senescence, apoptosis, and proliferation of fibroblasts. This inherent reparative function allows senescent cardiac fibroblasts to recover to a certain degree. Conversely, incomplete rescue of fibroblasts from senescence might lead to undesired fibrosis. We present new *in vitro* evidence suggesting that M2-like macrophages play a vital role in attenuating senescent and apoptotic fibroblasts through Nrg1/ErbB/PI3K/Akt signaling pathways. This contributes to various processes that are critical to mediate many aspects of cellular functions including cell growth and survival (Yu & Cui, 2016). However, further mechanistic studies are required to understand the signaling pathways downstream of these factors and the clear role of Nrg1 using both cardiac fibroblast-specific conditional *ErbB2/ErbB4*-knockout mice and macrophage-specific conditional *Nrg1*-knockout mice. Although this study focused on Nrg1-induced anti-apoptosis and anti-senescence of cardiac fibroblasts, M2-like macrophages are likely to mediate supplementary benefits in cardiac repair post-MI. These benefits may include reduced inflammation, activation of fibroblasts, and neovascular formation as shown in our previous study (Shiraishi et al., 2016). To develop potential therapies mediated by M2-like macrophages, future studies will also need to determine how the gene that encodes Nrg1 is switched on by MI and identify other molecules that regulate apoptosis, senescence, and proliferation of cardiac fibroblasts. Better understanding of the molecular mechanism in the healing process of MI and subsequent remodeling may reveal new treatment options.

In conclusion, our data provide evidence that the Nrg1/ErbB/PI3K/Akt signaling system critically regulates senescence and apoptosis of cardiac fibroblasts in the infarcted adult murine heart. This process might play a vital role in repair of the infarcted myocardium by regulating collagen synthesis (Fig 10). Therefore, this tissue repair mechanism controls the degree of rigidity and contraction of the infarcted heart, thereby determining the prognosis post-MI. Targeted activation of M2-like

macrophages might enhance this endogenous repair mechanism in senescent cardiac fibroblasts, which indicates that this approach may be a new therapeutic treatment for MI.

Methods

Animals. Eight- to 10-week-old mice were used in the experiments. C57BL/6 mice were purchased from Tokyo Laboratory Animals Science Co., Ltd. The mice were maintained in a specific pathogen-free room in our animal facility with a 12-hour light/dark cycle and free access to food and water. *In vitro* and *in vivo* experiments were performed in a blinded manner.

In vivo treatments. Mice were treated with three i.p. injections of 100 μg Trastuzumab (Bio X Cell; catalog BE0277) on the fourth, fifth, and sixth days after induction of myocardial infarction (MI). Samples were collected on the seventh, 12^{th}, and 28^{th} days after induction of MI.

Preparation of bone marrow-derived macrophages (BMDMs). Mouse BMDMs were prepared from the femurs and tibiae of 8-week-old wildtype (WT) mice as described previously (Shiraishi et al., 2016). Bone marrow mononuclear cells were collected by centrifugation on Ficoll-Paque (GE Healthcare) and were cultivated overnight in a CO_2 incubator in Dulbecco's modified Eagle's medium (DMEM; Sigma-Aldrich) containing 10% fetal bovine serum (FBS), 50 U/mL penicillin, 50 μg/mL streptomycin, and 10 ng/mL granulocyte-macrophage colony stimulating factor (R&D Systems; 415-ML). Unattached or weakly attached cells were collected and transferred to new dishes and cultivated for an additional 5 days. The cells were then prepared for coculture experiments.

Coculture of cardiac fibroblasts and BMDMs in a Boyden chamber. Cardiac fibroblasts (2×10^4) were plated on a 0.1% gelatin-coated 6-well dish (Thermo Scientific) and cultured for 48 hours in DMEM containing 10% FBS, 50 U/mL penicillin, and 50 μg/ mL streptomycin. Cardiac fibroblasts were damaged by 1 hour of treatment with 100 μM hydrogen peroxide (Sigma),as described previously (Bladier, Wolvetang et al., 1997) with some modifications. Then, the damaged fibroblasts were maintained in DMEM containing 10% FBS, 50 U/mL penicillin, and 50 μg/mL streptomycin. BMDMs (2×10^4) were seeded on polycarbonate membrane inserts (0.4 μm pore size; Thermo

Scientific) that were placed in wells containing fibroblasts. An anti-ErbB4 Ab (10 µg/mL; Thermo Scientific; catalog MA5-13016) was added to the culture medium at the beginning of the coculture.

Induction of myocardial infarction (MI). MI was induced in mice by ligating the left coronary artery under 2.0% isoflurane anesthesia and mechanical ventilation as described previously (Tano, Narita et al., 2014). Successful establishment of MI was confirmed by changes in the color and motion of the left ventricular walls. The survival rate and body weight change after MI were monitored daily.

Isolation of heart cells. Mouse heart cells were isolated as described previously (Shintani, Kapoor et al., 2013). Immediately after cervical dislocation, the aorta was clamped and cold Hank's balanced salt solution (HBSS; Sigma-Aldrich) was injected into the left ventricular cavity. The isolated hearts were cut into 1 mm^3 pieces, digested with 0.05% collagenase II (Sigma-Aldrich) at 37 °C for 15 minutes and then filtered through a 40-µm cell strainer (BD Falcon). The remnant heart tissues were digested again with a fresh digestion solution and similarly filtered. This cycle was repeated five times. The suspension obtained at each cycle was combined and subjected to flow cytometric analyses or fluorescence-activated cell sorting (FACS) after erythrocytes were depleted with Red Cell Lysis Buffer (BioLegend) in accordance with the manufacturer's protocol.

Flow cytometry and FACS. The isolated cells were resuspended in FACS buffer (HBSS with 2 mM EDTA and 0.5% BSA) and preincubated with an anti-mouse CD16/CD32 Ab (rat, 1:100 dilution; eBioscience; catalog 14-0161) to block Fc receptors. Dead cells and debris were excluded by forward scatter/side scatter and DAPI staining (1:1,000 dilution; Sigma-Aldrich). To determine phenotypes, the cells were stained with the following Abs for 3 hours at 4 °C: APC-conjugated anti-CD11b Ab (rat, 1:100 dilution; eBioscience; catalog 17-0112); phycoerythrin (PE)-conjugated anti-F4/80 Ab (rat, 1:20 dilution; eBioscience; catalog 12-4801), and Alexa Fluor 488-conjugated anti-CD206 Ab (rat, 1:50 dilution; BioLegend; catalog 141709). Cell sorting was performed with a FACSAria II (BD Biosciences).

Isolation of cardiac fibroblasts. Cardiac fibroblasts were isolated from Wistar rats (Charles River Laboratories) as described previously (Leicht, Greipel et al., 2000) with some modifications. The isolated rat heart was cut into 1 mm^3 pieces that were plated evenly in 0.1% gelatin-coated 10-cm dishes without contacting each other. Each fragment was covered by a droplet of DMEM containing

458 10% FBS, 50 U/ mL penicillin, and 50 µg/mL streptomycin and incubated for 24 hours at 37 °C in a
459 CO_2 incubator. Then, sufficient medium was added to cover the entire bottom of the culture dish, and
460 the culture was incubated for an additional 24 hours. After this period, sufficient medium was added
461 to completely cover the heart fragments and the culture was continued for an additional 5 days. When
462 fibroblast outgrowth was observed, the cells were collected by trypsinization. The fibroblasts were
463 maintained in DMEM containing 10% FBS, 50 U/mL penicillin, and 50 µg/mL streptomycin in 0.1%
464 gelatin-coated culture flasks. The cells were used at passage 3 or 4.
465 ***RNA extraction and real-time polymerase chain reaction (PCR).*** Total RNA was extracted from
466 cells or heart tissue with a Gene Jet PCR purification Kit (Thermo Scientific) and quantified with a
467 Nano-Drop 8000 spectrophotometer (Thermo Scientific). cDNA was synthesized using 25 and 150 ng
468 total RNAs from M2-macrophages and heart tissues, respectively, with a High-capacity cDNA
469 Reverse Transcription Kit (Applied Biosystems). Real-time PCR was performed by a QuantStudio
470 (Applied Biosystems) with SYBR Premix Ex Taq II (Takara Bio) under the following conditions:
471 95 °C for 30 seconds followed by 40 cycles at 95 °C for 5 seconds and 60 °C for 30 seconds. Gene
472 expression levels were normalized to *Gapdh* expression. The primers are shown in Supplemental
473 Table 1.
474 ***Microarray analysis.*** Total RNA of $CD206^+F4/80^+CD11b^+$ M2-like macrophages was isolated as
475 described above from the heart and peritoneal cavity, amplified with the RNA Amplification System
476 (NuGEN), and subjected to the Illumina bead array platform with a Mouse WG-6 v2.0 Expression
477 BeadChip (Illumina). Two independent biological replicates were prepared for each group category.
478 Median per chip normalization was performed in each array. We analyzed only genes whose signal
479 intensity was above 90 in one of the biological duplicates. A two-fold change cutoff was used to
480 identify differentially expressed genes.
481 ***Immunohistochemistry.*** Immediately after cervical dislocation, the aorta of the mouse was clamped
482 and ice-cold PBS was injected into the left ventricular cavity. The mouse heart was then perfused with
483 ice-cold 4% paraformaldehyde in PBS. The heart was removed, cut at the midpoint along the short
484 axis of left ventricle, embedded in optimal cutting temperature compound (VWR International), and
485 frozen in isopentane chilled in liquid nitrogen. Frozen tissue sections (8 µm thick) were prepared and

non-specific antibody-binding sites were pre-blocked with blocking buffer (PBS containing 5% goat serum). Then, primary antibodies were applied overnight at 4 °C. After rinsing three times for 15 minutes in PBS, the sections were incubated with appropriate fluorophore-conjugated secondary antibodies and 4□,6-diamidino-2-phenylindole (DAPI) (Sigma-Aldrich, D9542) in blocking buffer for 1 hour at room temperature. Stained sections were mounted with DAKO Fluorescence Mounting Medium (Agilent, S302380-2). The primary and secondary antibodies used in this study are shown in Supplemental Table 2.

Picrosirius red staining. Frozen tissue sections (8 µm thick) were incubated in 1.5% phosphomolybdic acid for 60 minutes, 0.1% Picrosirius Red for 15 minutes, and then a 0.5% acetic acid solution for 3 minutes. After dehydration by adding increasing concentrations of ethanol to xylene, the sections were mounted with DPX mounting medium (VWR International). The infarct area was defined as the area with loss of more than 90% cardiomyocytes.

Masson trichrome staining. Frozen tissue sections (8 µm thick) were prepared as described above and stained using a Trichrome Stain Kit (Scy Tek Laboratories) in accordance with the manufacturer's instructions.

Immunocytochemistry. Cells were fixed in 4% paraformaldehyde/PBS for 5 minutes at room temperature. Apart from cells used for surface antigen staining, cells were incubated in PBS containing 0.1% of Triton X-100 for 5 minutes at room temperature. Non-specific antibody binding sites were pre-blocked with PBS containing 5% goat serum for 30 minutes at room temperature. Then, primary antibodies were applied to the cells for 1 hour at room temperature. The primary antibodies were as follows: anti-vimentin (1:100, Abcam, ab24525), anti-cleaved caspase 3 (1:100, Cell Signaling, 9661), anti-Ki-67 (1:100, eBioscience, 14-5698), and anti-αSMA (1:00, Abcam, ab5694). After rinsing, the cells were incubated with fluorophore-conjugated secondary antibodies (1:300, Alexa Fluor 488- or 594-conjugated polyclonal, Invitrogen) and DAPI in blocking buffer for 1 hour at room temperature.

Imaging and analysis. Digital images were acquired under an All-in-One microscope (BZ-8000; KEYENCE). Image analyses were performed by importing images as TIFF files into ImageJ software (National Institute of Health). To quantify fibrin formation, the fibrin area was quantified as the

514 percentage of the fibrin-positive area in the whole image. Images were acquired at five independent
515 regions and analyzed. The color threshold function of ImageJ was applied to measure macrophages,
516 fibroblasts, the fibrin clot area, and cell size of cultured fibroblasts.
517 ***Immunoblotting.*** For western blot analysis, tissue was frozen, crushed, and then lysed in T-PER
518 Tissue Protein Extraction Regent (Thermo Scientific, 78510) in accordance with the manufacturer's
519 protocol. The protein concentration was measured with the Nano-Drop 8000 spectrophotometer and
520 lysates containing 50 μg protein each were separated by PAGE, transferred onto a polyvinylidene
521 difluoride membrane, and then analyzed by immunoblotting using the primary and second
522 antibodies shown in the Supplemental Table 3. Protein bands were visualized with a Super Signal
523 West Pico Substrate (Thermo Scientific, 34077) in accordance with the manufacturer's instructions.
524 ***Statistics.*** All statistical tests were performed with GraphPad Prism software version 8 (GraphPad
525 Software). Data represent the mean ± SEM. For comparisons between multiple groups,
526 repeated-measures analysis of variance (ANOVA) or one- or two-way ANOVA was performed,
527 followed by Bonferroni's post-hoc test. Two groups were compared with the two-tailed, unpaired
528 Student's *t*-test. Cardiac rupture rates were compared by the χ^2 test and survival curves were
529 compared by the log-rank test.
530
531 **Data availability**
532
533 Microarray data: Gene Expression Omnibus GSE69879
534 (https://www.ncbi.nlm.nih.gov/geo/query/acc.cgi?acc=GSE69879)
535
536 **Acknowledgments**
537
538 This project was funded by the Uehara Memorial Foundation, SENSHIN Medical Research
539 Foundation, a Grant-in-Aid for Scientific Research (C), the Mochida Memorial Foundation for
540 Medical and Pharmaceutical Research, Takeda Science Foundation, and Public Trust Surgery

Research Fund. We thank Ellen Knapp, PhD, and Mitchell Arico from Edanz Group (https://en-author-services.edanz.com/ac) for editing a draft of this manuscript.

Author contributions

MS and KS conceived and designed the study. MS conducted most of the experiments and acquired the data with support from AY and KS. All authors participated in the analysis and interpretation of the data. MS and KS primarily wrote and edited the manuscript with input from all other authors.

Conflict of interest statement

The authors have declared that no conflicts of interest exist.

References

Acosta JC, Banito A, Wuestefeld T, Georgilis A, Janich P, Morton JP, Athineos D, Kang TW, Lasitschka F, Andrulis M, Pascual G, Morris KJ, Khan S, Jin H, Dharmalingam G, Snijders AP, Carroll T, Capper D, Pritchard C, Inman GJ et al. (2013) A complex secretory program orchestrated by the inflammasome controls paracrine senescence. *Nat Cell Biol* 15: 978-90

Alam P, Haile B, Arif M, Pandey R, Rokvic M, Nieman M, Maliken BD, Paul A, Wang YG, Sadayappan S, Ahmed RPH, Kanisicak O (2019) Inhibition of Senescence-Associated Genes Rb1 and Meis2 in Adult Cardiomyocytes Results in Cell Cycle Reentry and Cardiac Repair Post-Myocardial Infarction. *J Am Heart Assoc* 8: e012089

Alcorta DA, Xiong Y, Phelps D, Hannon G, Beach D, Barrett JC (1996) Involvement of the cyclin-dependent kinase inhibitor p16 (INK4a) in replicative senescence of normal human fibroblasts. *Proc Natl Acad Sci U S A* 93: 13742-7

Aurora AB, Porrello ER, Tan W, Mahmoud AI, Hill JA, Bassel-Duby R, Sadek HA, Olson EN (2014) Macrophages are required for neonatal heart regeneration. *J Clin Invest* 124: 1382-92

Baliga RR, Pimental DR, Zhao YY, Simmons WW, Marchionni MA, Sawyer DB, Kelly RA (1999) NRG-1-induced cardiomyocyte hypertrophy. Role of PI-3-kinase, p70(S6K), and MEK-MAPK-RSK. *Am J Physiol* 277: H2026-37

Bersell K, Arab S, Haring B, Kuhn B (2009) Neuregulin1/ErbB4 signaling induces cardiomyocyte proliferation and repair of heart injury. *Cell* 138: 257-70

Bladier C, Wolvetang EJ, Hutchinson P, de Haan JB, Kola I (1997) Response of a primary human fibroblast cell line to H2O2: senescence-like growth arrest or apoptosis? *Cell Growth Differ* 8: 589-98

Childs BG, Durik M, Baker DJ, van Deursen JM (2015) Cellular senescence in aging and age-related disease: from mechanisms to therapy. *Nat Med* 21: 1424-35

578 Childs BG, Li H, van Deursen JM (2018) Senescent cells: a therapeutic target for
579 cardiovascular disease. *J Clin Invest* 128: 1217-1228
580 Coppe JP, Desprez PY, Krtolica A, Campisi J (2010) The senescence-associated secretory
581 phenotype: the dark side of tumor suppression. *Annu Rev Pathol* 5: 99-118
582 Deng C, Zhang P, Harper JW, Elledge SJ, Leder P (1995) Mice lacking p21CIP1/WAF1
583 undergo normal development, but are defective in G1 checkpoint control. *Cell* 82: 675-84
584 Dickstein K, Cohen-Solal A, Filippatos G, McMurray JJ, Ponikowski P, Poole-Wilson PA,
585 Stromberg A, van Veldhuisen DJ, Atar D, Hoes AW, Keren A, Mebazaa A, Nieminen M,
586 Priori SG, Swedberg K, Guidelines ESCCfP (2008) ESC Guidelines for the diagnosis and
587 treatment of acute and chronic heart failure 2008: the Task Force for the Diagnosis and
588 Treatment of Acute and Chronic Heart Failure 2008 of the European Society of Cardiology.
589 Developed in collaboration with the Heart Failure Association of the ESC (HFA) and endorsed
590 by the European Society of Intensive Care Medicine (ESICM). *Eur Heart J* 29: 2388-442
591 ElZarrad MK, Mukhopadhyay P, Mohan N, Hao E, Dokmanovic M, Hirsch DS, Shen Y,
592 Pacher P, Wu WJ (2013) Trastuzumab alters the expression of genes essential for cardiac
593 function and induces ultrastructural changes of cardiomyocytes in mice. *PLoS One* 8: e79543
594 Fuller SJ, Sivarajah K, Sugden PH (2008) ErbB receptors, their ligands, and the consequences
595 of their activation and inhibition in the myocardium. *J Mol Cell Cardiol* 44: 831-54
596 Gelb BD, Tartaglia M (2011) RAS signaling pathway mutations and hypertrophic
597 cardiomyopathy: getting into and out of the thick of it. *J Clin Invest* 121: 844-7
598 Gemberling M, Karra R, Dickson AL, Poss KD (2015) Nrg1 is an injury-induced
599 cardiomyocyte mitogen for the endogenous heart regeneration program in zebrafish. *Elife* 4
600 Gould KE, Taffet GE, Michael LH, Christie RM, Konkol DL, Pocius JS, Zachariah JP,
601 Chaupin DF, Daniel SL, Sandusky GE, Jr., Hartley CJ, Entman ML (2002) Heart failure and
602 greater infarct expansion in middle-aged mice: a relevant model for postinfarction failure. *Am J*
603 *Physiol Heart Circ Physiol* 282: H615-21
604 Hayakawa K, Takemura G, Kanoh M, Li Y, Koda M, Kawase Y, Maruyama R, Okada H,
605 Minatoguchi S, Fujiwara T, Fujiwara H (2003) Inhibition of granulation tissue cell apoptosis
606 during the subacute stage of myocardial infarction improves cardiac remodeling and
607 dysfunction at the chronic stage. *Circulation* 108: 104-9
608 Hedhli N, Huang Q, Kalinowski A, Palmeri M, Hu X, Russell RR, Russell KS (2011)
609 Endothelium-derived neuregulin protects the heart against ischemic injury. *Circulation* 123:
610 2254-62
611 Ikeda N, Asano K, Kikuchi K, Uchida Y, Ikegami H, Takagi R, Yotsumoto S, Shibuya T,
612 Makino-Okamura C, Fukuyama H, Watanabe T, Ohmuraya M, Araki K, Nishitai G, Tanaka M
613 (2018) Emergence of immunoregulatory Ym1(+)Ly6C(hi) monocytes during recovery phase
614 of tissue injury. *Sci Immunol* 3
615 Kirabo A, Ryzhov S, Gupte M, Sengsayadeth S, Gumina RJ, Sawyer DB, Galindo CL (2017)
616 Neuregulin-1beta induces proliferation, survival and paracrine signaling in normal human
617 cardiac ventricular fibroblasts. *J Mol Cell Cardiol* 105: 59-69
618 Krizhanovsky V, Yon M, Dickins RA, Hearn S, Simon J, Miething C, Yee H, Zender L, Lowe
619 SW (2008) Senescence of activated stellate cells limits liver fibrosis. *Cell* 134: 657-67
620 Kuramochi Y, Cote GM, Guo X, Lebrasseur NK, Cui L, Liao R, Sawyer DB (2004) Cardiac
621 endothelial cells regulate reactive oxygen species-induced cardiomyocyte apoptosis through
622 neuregulin-1beta/erbB4 signaling. *J Biol Chem* 279: 51141-7
623 Leicht M, Greipel N, Zimmer H (2000) Comitogenic effect of catecholamines on rat cardiac
624 fibroblasts in culture. *Cardiovasc Res* 48: 274-84
625 Lemmens K, Doggen K, De Keulenaer GW (2007) Role of neuregulin-1/ErbB signaling in
626 cardiovascular physiology and disease: implications for therapy of heart failure. *Circulation*
627 116: 954-60

628 Long X, Boluyt MO, Hipolito ML, Lundberg MS, Zheng JS, O'Neill L, Cirielli C, Lakatta EG,
629 Crow MT (1997) p53 and the hypoxia-induced apoptosis of cultured neonatal rat cardiac
630 myocytes. *J Clin Invest* 99: 2635-43
631 Meyer D, Yamaai T, Garratt A, Riethmacher-Sonnenberg E, Kane D, Theill LE, Birchmeier C
632 (1997) Isoform-specific expression and function of neuregulin. *Development* 124: 3575-86
633 Munoz-Espin D, Serrano M (2014) Cellular senescence: from physiology to pathology. *Nat*
634 *Rev Mol Cell Biol* 15: 482-96
635 Olayioye MA, Neve RM, Lane HA, Hynes NE (2000) The ErbB signaling network: receptor
636 heterodimerization in development and cancer. *EMBO J* 19: 3159-67
637 Park S, Jiang Z, Mortenson ED, Deng L, Radkevich-Brown O, Yang X, Sattar H, Wang Y,
638 Brown NK, Greene M, Liu Y, Tang J, Wang S, Fu YX (2010) The therapeutic effect of
639 anti-HER2/neu antibody depends on both innate and adaptive immunity. *Cancer Cell* 18:
640 160-70
641 Pascual-Gil S, Abizanda G, Iglesias E, Garbayo E, Prosper F, Blanco-Prieto MJ (2019) NRG1
642 PLGA MP locally induce macrophage polarisation toward a regenerative phenotype in the
643 heart after acute myocardial infarction. *J Drug Target* 27: 573-581
644 Polizzotti BD, Ganapathy B, Walsh S, Choudhury S, Ammanamanchi N, Bennett DG, dos
645 Remedios CG, Haubner BJ, Penninger JM, Kuhn B (2015) Neuregulin stimulation of
646 cardiomyocyte regeneration in mice and human myocardium reveals a therapeutic window. *Sci*
647 *Transl Med* 7: 281ra45
648 Polyak K, Xia Y, Zweier JL, Kinzler KW, Vogelstein B (1997) A model for p53-induced
649 apoptosis. *Nature* 389: 300-5
650 Sasaki M, Miyakoshi M, Sato Y, Nakanuma Y (2010) Modulation of the microenvironment by
651 senescent biliary epithelial cells may be involved in the pathogenesis of primary biliary
652 cirrhosis. *J Hepatol* 53: 318-25
653 Serrano M, Lin AW, McCurrach ME, Beach D, Lowe SW (1997) Oncogenic ras provokes
654 premature cell senescence associated with accumulation of p53 and p16INK4a. *Cell* 88:
655 593-602
656 Sharpless NE, Sherr CJ (2015) Forging a signature of in vivo senescence. *Nat Rev Cancer* 15:
657 397-408
658 Shih H, Lee B, Lee RJ, Boyle AJ (2011) The aging heart and post-infarction left ventricular
659 remodeling. *J Am Coll Cardiol* 57: 9-17
660 Shinde AV, Frangogiannis NG (2014) Fibroblasts in myocardial infarction: a role in
661 inflammation and repair. *J Mol Cell Cardiol* 70: 74-82
662 Shintani Y, Kapoor A, Kaneko M, Smolenski RT, D'Acquisto F, Coppen SR, Harada-Shoji N,
663 Lee HJ, Thiemermann C, Takashima S, Yashiro K, Suzuki K (2013) TLR9 mediates cellular
664 protection by modulating energy metabolism in cardiomyocytes and neurons. *Proc Natl Acad*
665 *Sci U S A* 110: 5109-14
666 Shiraishi M, Shintani Y, Shintani Y, Ishida H, Saba R, Yamaguchi A, Adachi H, Yashiro K,
667 Suzuki K (2016) Alternatively activated macrophages determine repair of the infarcted adult
668 murine heart. *J Clin Invest* 126: 2151-66
669 Stein GH, Drullinger LF, Soulard A, Dulic V (1999) Differential roles for cyclin-dependent
670 kinase inhibitors p21 and p16 in the mechanisms of senescence and differentiation in human
671 fibroblasts. *Mol Cell Biol* 19: 2109-17
672 Suzuki T, Arumugam P, Sakagami T, Lachmann N, Chalk C, Sallese A, Abe S, Trapnell C,
673 Carey B, Moritz T, Malik P, Lutzko C, Wood RE, Trapnell BC (2014) Pulmonary macrophage
674 transplantation therapy. *Nature* 514: 450-4
675 Takemura G, Ohno M, Hayakawa Y, Misao J, Kanoh M, Ohno A, Uno Y, Minatoguchi S,
676 Fujiwara T, Fujiwara H (1998) Role of apoptosis in the disappearance of infiltrated and
677 proliferated interstitial cells after myocardial infarction. *Circ Res* 82: 1130-8

Tano N, Narita T, Kaneko M, Ikebe C, Coppen SR, Campbell NG, Shiraishi M, Shintani Y, Suzuki K (2014) Epicardial placement of mesenchymal stromal cell-sheets for the treatment of ischemic cardiomyopathy; in vivo proof-of-concept study. *Mol Ther* 22: 1864-71

Uray IP, Connelly JH, Thomazy V, Shipley GL, Vaughn WK, Frazier OH, Taegtmeyer H, Davies PJ (2002) Left ventricular unloading alters receptor tyrosine kinase expression in the failing human heart. *J Heart Lung Transplant* 21: 771-82

van den Borne SW, Diez J, Blankesteijn WM, Verjans J, Hofstra L, Narula J (2010) Myocardial remodeling after infarction: the role of myofibroblasts. *Nat Rev Cardiol* 7: 30-7

van Deursen JM (2014) The role of senescent cells in ageing. *Nature* 509: 439-46

Vermeulen Z, Hervent AS, Dugaucquier L, Vandekerckhove L, Rombouts M, Beyens M, Schrijvers DM, De Meyer GRY, Maudsley S, De Keulenaer GW, Segers VFM (2017) Inhibitory actions of the NRG-1/ErbB4 pathway in macrophages during tissue fibrosis in the heart, skin, and lung. *Am J Physiol Heart Circ Physiol* 313: H934-H945

Wang YA, Elson A, Leder P (1997) Loss of p21 increases sensitivity to ionizing radiation and delays the onset of lymphoma in atm-deficient mice. *Proc Natl Acad Sci U S A* 94: 14590-5

Yu JS, Cui W (2016) Proliferation, survival and metabolism: the role of PI3K/AKT/mTOR signalling in pluripotency and cell fate determination. *Development* 143: 3050-60

Yutzey KE (2015) Regenerative biology: Neuregulin 1 makes heart muscle. *Nature* 520: 445-6

Zhu F, Li Y, Zhang J, Piao C, Liu T, Li HH, Du J (2013) Senescent cardiac fibroblast is critical for cardiac fibrosis after myocardial infarction. *PLoS One* 8: e74535

Figure legends

Figure 1. ***Cardiac fibroblasts undergo apoptosis and senescence after MI.***

A. Double immunofluorescence staining of Thy1 and cleaved caspase 3 (CC-3) demonstrated that apoptosis of cardiac fibroblasts in the infarct area was exacerbated at post-myocardial infarction (MI) days 7 and 28 compared with the remote area. Scale bars: 100 μm. $n = 4$ in each group.

B. SA-β-gal staining demonstrated that spindle-shaped senescent fibroblasts had accumulated in the infarct area. Scale bars: 100 μm.

C. Quantitative reverse transcription-polymerase chain reaction analysis showed post-MI upregulation of senescence-associated genes in the infarct area at post-MI day 7 compared with the non-MI heart (day 0). $n = 4$ in each group. Data represent the mean ± SEM. $^{*}P < 0.05$, $^{**}P < 0.01$, $^{***}P < 0.005$ versus the remote area; $^{\#}P < 0.05$, $^{\#\#}P < 0.01$, $^{\#\#\#}P < 0.005$ versus the non-MI heart; one-way ANOVA.

Figure 2. ***Nrg1 expression upregulates in the infarcted myocardium, while cardiac fibroblasts express Nrg1 receptors.***

715 A. qRT-PCR analysis confirmed post-MI upregulation of *Nrg1*. Expression levels relative to the intact
716 heart are presented. $n = 4$ in each group.
717 B. Immunohistochemistry demonstrated that the ratios of $ErbB2^+$ and $ErbB4^+$ fibroblasts (percentage
718 of $Thy1^+ErbB2/4^+$ myofibroblasts/percentage of $Thy1^+$ fibroblasts) were markedly increased in the
719 post-MI heart. Scale bars: 100 μm. $n = 4$ in each group. Data represent the mean ± SEM. $^*P < 0.05$,
720 $^{**}P < 0.01$, $^{***}P < 0.005$ versus the remote area; $^{\#}P < 0.05$, $^{\#\#}P < 0.01$, $^{\#\#\#}P < 0.005$ versus the
721 non-MI heart; one-way ANOVA.
722
723 **Figure 3.** ***M2-like macrophages accumulate in the infarct and express Nrg1.***
724 A. Immunohistochemistry showed that accumulation of $CD206^+$ M2-like macrophages was increased
725 in the infarcted area with a post-myocardial infarction (MI) peak on day 7. Scale bars: 100 μm. $n =$
726 4 in each group. Data represent the mean ± SEM. $^*P < 0.05$, $^{**}P < 0.01$, $^{***}P < 0.005$ versus the
727 remote area; $^{\#}P < 0.05$, $^{\#\#}P < 0.01$, $^{\#\#\#}P < 0.005$ versus the non-MI heart; one-way ANOVA.
728 B. Flow cytometric analysis confirmed that $CD206^+F4/80^+CD11b^+$ M2-like macrophages were
729 present in normal, non-myocardial infarction (non-MI), and day 7 post-MI hearts of adult
730 C57BL/6 mice. $n = 6$ in each group.
731 C. Microarray analysis demonstrated that M2 macrophages after myocardial infarction (M2: MI) had
732 a different expression profile from that of M2: non-MI macrophages. Scatter plot revealed that 70
733 genes were upregulated and 39 were downregulated in M2: MI macrophages compared with M2:
734 non-MI macrophages. The upregulated genes included neuregulin 1 (*Nrg1*).
735 D. Quantitative reverse transcription-polymerase chain reaction analysis confirmed post-MI
736 upregulation of *Nrg1* in $CD206^+F4/80^+CD11b^+$ cardiac M2-like macrophages [M2: MI]. $n = 4$ in
737 each group. Data represent the mean ± SEM. $^{\#}P < 0.05$, $^{\#\#}P < 0.01$, $^{\#\#\#}P < 0.005$ versus M2:
738 non-MI macrophages; two-tailed, unpaired Student's *t*-test.
739 E. Double immunofluorescence staining of $CD206^+$ M2-like macrophages and neuregulin 1 (Nrg1)
740 demonstrated Nrg1 expression on the surface of $CD206^+$ M2-like macrophages. Scale bars: 100
741 μm. $n = 4$ in each group.
742

Figure 4. ***Bone marrow-derived macrophages attenuate H_2O_2-induced apoptosis and senescence of cardiac fibroblasts via Nrg1 secretion.***

A. Representative images from phase-contrast microscopy. Treatment with a hydrogen peroxide (H_2O_2) solution changed the spindle-shaped appearance to a significantly enlarged, flattened morphology. After addition of bone marrow-derived macrophages (BMDMs), fibroblasts returned to the spindle-shaped morphology. After addition of an anti-ErbB antibody (Ab), fibroblasts displayed the same gross morphology as senescent fibroblasts treated with H_2O_2. Recombinant neuregulin 1 (Nrg1) similarly changed the gross morphology to a spindle shape. Scale bars: 100 μm. $n = 4$ in each group.

B. SA-β-gal staining showed that senescence of fibroblasts was exacerbated in coculture with H_2O_2, but not with H_2O_2 and BMDMs. This suppression of senescence was attenuated by coculture with the anti-ErbB Ab. Nrg1 suppressed fibroblast senescence. Scale bars: 100 μm. $n = 4$ in each group

C. Apoptosis of cardiac fibroblasts (ratio of cleaved caspase 3^+DAPI^+ fibroblasts to $DAPI^+$ fibroblasts) was increased in coculture with H_2O_2, but decreased in cardiac fibroblasts cocultured with BMDMs. This decrease in apoptosis was eliminated by the anti-ErbB Ab. Nrg1 suppressed apoptosis. Nuclei were counterstained with 4□,6-diamidino-2-phenylindole (DAPI). $n = 4$ in each group. Scale bars: 100 μm.

D. Proliferation of cardiac fibroblasts (ratio of $Ki\text{-}67^+$ and $DAPI^+$ fibroblasts to $DAPI^+$ fibroblasts) was decreased in cocultures with H_2O_2, but increased in cardiac fibroblasts cocultured BMDMs. This increase in proliferation was eliminated by the anti-ErbB Ab. Nrg1 accelerated proliferation. Nuclei were counterstained with DAPI. Scale bars: 50 μm. $n = 4$ in each group. Data represent the mean ± SEM. $^{\#}P < 0.05$ versus control, $^{*}P < 0.05$ versus H_2O_2, $^{‡}P < 0.05$ versus H_2O_2+BMDMs, $^{†}P < 0.05$ versus H_2O_2+BMDMs+Ab, $^{§}P < 0.05$ versus H_2O_2+Nrg1; one-way ANOVA.

Figure 5. ***BMDMs promote fibroblast activation and collagen synthesis.***

A–C. Representative images of immunocytochemical staining for (A) vimentin and αSMA, (B) vimentin and collagen I, and (C) vimentin and collagen III. The staining was performed at 48 hours after the start of culture.

A. Activation of cardiac fibroblasts (ratio of vimentin$^+$ and αSMA$^+$ myofibroblasts to vimentin$^+$ fibroblasts) was equal in cocultures with hydrogen peroxide (H_2O_2), but markedly increased in cardiac fibroblasts cocultured with bone marrow-derived macrophages (BMDMs). This increase in activation was accelerated by the anti-ErbB antibody (Ab). Addition of recombinant neuregulin 1 (Nrg1) did not affect activation of cardiac fibroblasts. Scale bars: 100 μm. n = 4 in each group.

B. Collagen I synthesis was equal in cocultures with H_2O_2, but significantly increased in cardiac fibroblasts cocultured with BMDMs. This increase in production was enhanced by the anti-ErbB Ab. Addition of Nrg1 did not affect collagen I synthesis. Scale bars: 100 μm. n = 4 in each group.

C. Collagen III synthesis exhibited a similar tendency as collagen I synthesis. Scale bars: 100 μm. n = 4 in each group. Data represent the mean ± SEM. $^{\#}P < 0.05$ versus control, $^{*}P < 0.05$ versus H_2O_2, $^{\ddagger}P < 0.05$ versus H_2O_2+BMDMs, $^{\dagger}P < 0.05$ versus H_2O_2+BMDMs+Ab, $^{\S}P < 0.05$ versus H_2O_2+Nrg1; one-way ANOVA.

Figure 6. ***PI3K/Akt signaling pathway is associated with BMDM-attenuated apoptosis and senescence of cardiac fibroblasts through Nrg1.***

A. Representative bands of PI3K, pPI3K, Akt, pAkt, and β-actin in cardiac fibroblasts at 48 hours after coculture with or without hydrogen peroxide (H_2O_2)/bone marrow-derived macrophages (BMDMs)/anti-ErbB antibody (Ab)/recombinant neuregulin 1 (Nrg1). Bar graph shows quantification of relative pPI3k/PI3k and pAkt/Akt. H_2O_2 alone did not affect activation of PI3K/AKT signaling in fibroblasts. Addition of BMDMs significantly activated the signaling pathway and addition of the anti-ErbB Ab impaired the activation. Addition of Nrg1 re-stimulated the signaling pathway. n = 4 in each group.

B. Quantitative reverse transcription-polymerase chain reaction analysis of cardiac fibroblasts at 48 hours after coculture with or without H_2O_2/BMDMs/anti-ErbB Ab/Nrg1. The expression levels of

795 senescence-associated genes (*p53*, *p21*, *p16*, and *SA-β-gal*) were increased in cocultures with H_2O_2
796 with a time lapse, but decreased in cocultures with BMDMs. Addition of the anti-ErbB Ab
797 increased such expression and addition of Nrg1 suppressed it. $n = 4$ in each group.
798 C. Expression levels of cell cycle-associated genes (*Cdk4*, *Cdk6*, *Cdk2*, and *Ki-67*) were suppressed in
799 cocultures with H_2O_2, but recovered in cocultures with BMDMs. Addition of the anti-ErbB Ab
800 decreased such expression and addition of Nrg1 recovered the expression. $n = 4$ in each group.
801 D. Expression of the p53 suppressor gene (*MDM2*) was significantly increased in coculture with
802 BMDMs. $n = 4$ in each group.
803 E. Expression levels of cell survival-associated gene (*mTOR*) were suppressed in cocultures with
804 H_2O_2, but recovered in cocultures with BMDMs. Addition of the anti-ErbB Ab re-suppressed the
805 expression and addition of Nrg1 increased it again.
806 F. Expression of senescence-associated secretory phenotype-associated gene (*IL-6*) was significantly
807 increased in cocultures with BMDMs and after addition of the anti-ErbB Ab. $n = 4$ in each group.
808 Data represent the mean ± SEM. $^{\#}P < 0.05$ versus control, $^{*}P < 0.05$ versus H_2O_2, $^{\ddagger}P < 0.05$ versus
809 H_2O_2+BMDMs, $^{\dagger}P < 0.05$ versus H_2O_2+BMDMs+Ab, $^{\S}P < 0.05$ versus H_2O_2+Nrg1; one-way
810 ANOVA.
811 G. Schematic representation and overview of the Nrg1/PI3K/AKT pathway. Ischemia contributes to
812 the development of cellular damage, which leads to senescence, cell cycle arrest, and apoptosis.
813 Nrg1 binding to coreceptor ErbB2/ErbB4 leads to activation of PI3K/AKT and inactivation of p53
814 and p21. Arrowheads indicate stimulation, whereas hammerheads represent inhibition.
815
816 **Figure 7.** ***In vivo inhibition of Nrg1 signaling promotes apoptosis and senescence of cardiac***
817 ***fibroblasts.***
818 A–C. Quantitative reverse transcription-polymerase chain reaction analysis showed post-myocardial
819 infarction (MI) upregulation of (A) apoptosis-associated gene *Casp3* and (B and C)
820 senescence-associated genes (*SA-β-gal*, *p53*, *p21*, and *p16*) in mice after intraperitoneal
821 trastuzumab injection compared with controls. $n = 4$ in each group.

D. Double immunofluorescence staining of Thy1 and cleaved caspase 3 (CC-3) demonstrated that the ratio of apoptotic cardiac fibroblasts in the infarct area was increased in mice after intraperitoneal trastuzumab injection compared with controls at post-myocardial infarction (MI) days 7, 14, and 28. Arrow shows $Thy1^{+}CC\text{-}3^{+}$ cells. Scale bars: 100 μm. $n = 4$ in each group.

E. SA-β-gal staining demonstrated that senescence of cardiac cells in the infarct area was exacerbated in mice after intraperitoneal trastuzumab injection compared with controls at post-myocardial infarction (MI) days 7 and 14. Scale bars: 20 μm. $n = 4$ in each group. Data represent the mean ± SEM. $^{*}P < 0.05$, $^{**}P < 0.01$, $^{***}P < 0.005$ versus each group; $^{\#}P < 0.05$, $^{\#\#}P < 0.01$, $^{\#\#\#}P < 0.005$ versus the non-MI heart; one-way ANOVA.

Figure 8. ***In vivo inhibition of Nrg1 signaling activates cardiac fibroblasts and exacerbates fibrosis.***

A. Masson trichrome staining demonstrated that deposition of collagen fibrils was increased in the post-MI infarct area with a time lapse. Intraperitoneal trastuzumab injection significantly increased collagen fibrils in the infarct area. Scale bars: 100 μm. $n = 4$ in each group.

B. Double immunofluorescence staining of Thy1 and αSMA showed increased accumulation and activation of cardiac fibroblasts in the infarct area in the trastuzumab group compared with the control group. Scale bars: 100 μm. $n = 4$ in each group.

C. Quantitative reverse transcription-polymerase chain reaction (qRT-PCR) analysis showed post-MI upregulation of fibrosis-associated genes (*αSMA*, *Col1a1*, and *Col3a1*) in mice after intraperitoneal trastuzumab injection compared with controls. $n = 4$ in each group. Data represent the mean ± SEM. $^{*}P < 0.05$, $^{**}P < 0.01$, $^{***}P < 0.005$ versus each group; $^{\#}P < 0.05$, $^{\#\#}P < 0.01$, $^{\#\#\#}P < 0.005$ versus the non-MI heart; one-way ANOVA.

Figure 9. ***In vivo inhibition of Nrg1 signaling exacerbates myocardial inflammation and promotes accumulation of M2-like macrophages.***

A. Quantitative reverse transcription-polymerase chain reaction analysis showed post-myocardial infarction (MI) upregulation of senescence-associated secretory phenotype-associated genes (CCl3,

849 *IL-6*, and *TNF*) in mice after intraperitoneal trastuzumab injection compared with controls. $n = 4$ in
850 each group.
851 B. Immunohistochemistry showed increased accumulation of $CD206^+$ M2-like macrophages in the
852 infarct area with a post-myocardial infarction (MI) peak on day 7. Intraperitoneal trastuzumab
853 injection significantly accelerated accumulation of $CD206^+$ M2-like macrophages in the infarct
854 area. Scale bars: 100 μm. $n = 4$ in each group. Data represent the mean ± SEM. $^*P < 0.05$, $^{**}P <$
855 0.01, $^{***}P < 0.005$ versus each group; $^{\#}P < 0.05$ $^{\#\#}P < 0.01$, $^{\#\#\#}P < 0.005$ versus the non-MI heart;
856 one-way ANOVA.
857
858 **Figure 10. Schematic illustration of the inter-relationship between M2-like macrophages and**
859 **cardiac fibroblasts.**
860 Ischemic injury contributes to the development of cellular senescence and apoptosis. Senescent
861 cells, including cardiac fibroblasts, show the senescence-associated secretory phenotype (SASP),
862 which activate M2-like macrophages. M2-like macrophages suppress senescence and apoptosis of
863 fibroblasts and simultaneously accelerate proliferation. Osteopontin-mediated induction of
864 fibroblasts into myofibroblasts promotes fibrosis (11).
865
866 **Expanded View Figure legends**
867
868 **Expanded View Figure 1.** ***Myocardial infarction promotes activation of cardiac fibroblasts and***
869 ***exacerbates inflammation.***
870 A. Masson trichrome staining showed that deposition of collagen fibrils was increased in the infarct
871 area with a time lapse after myocardial infarction (MI). Scale bars: 100 μm. $n = 4$ in each group.
872 B. Quantitative reverse transcription-polymerase chain reaction analysis (qRT-PCR) analysis showed
873 post-MI upregulation of fibrosis-associated genes in the infarct area at post-MI day 7 compared
874 with the non-MI heart (day 0). $n = 4$ in each group.
875 C. Immunohistochemistry showed that accumulation of $Thy1^+$ fibroblasts was increased in the infarct
876 area with a post-myocardial infarction (MI) peak on day 7. Scale bars: 100 μm. n=4 in each group.

D. Activated cardiac fibroblasts ($Thy1^+$ and αSMA^+ fibroblasts) were significantly increased in the infarct area with a post-MI peak on day 7. Scale bars: 100 μm. n=4 in each group.

E. qRT-PCR analysis showed post-MI upregulation of inflammatory genes in the infarct area at post-MI day 7 compared with the non-MI heart (day 0). $n = 4$ in each group. Data represent the mean ± SEM. $^*P < 0.05$, $^{**}P < 0.01$, $^{***}P < 0.005$ versus the remote area; $^{\#}P < 0.05$, $^{\#\#}P < 0.01$, $^{\#\#\#}P < 0.005$ versus the non-MI heart; one-way analysis of variance (ANOVA).

Expanded View Figure 2. ***Cardiac M2-like macrophages strengthen their reparative ability.***

A. $CD206^+F4/80^+CD11b^+$ M2-like macrophages were isolated from intact hearts [non-MI (M2)] and day 7 post-MI hearts [MI (M2)] by fluorescence-activated cell sorting and subjected to microarray analysis. Macrophages from different origins showed distinct molecular signatures.

B. Signal intensity revealed that, among genes encoding secreted proteins, 13 were upregulated and three were downregulated in MI (M2) macrophages compared with non-MI (M2) macrophages. The upregulated genes included anti-inflammatory and anti-apoptotic genes as well as genes associated with cell survival and tissue repair.

C. Gene set enrichment analysis showed that $CD206^+F4/80^+CD11b^+$ M2-like macrophages in the post-MI heart were significantly relevant to regulation of cell survival.

Expanded View Figure 3. ***H_2O_2 induces apoptosis and senescence of cardiac fibroblasts.***

A. Schematic of the coculture protocol. Hydrogen peroxide (H_2O_2)-treated cardiac fibroblasts were cocultured with or without bone marrow-derived macrophages (BMDMs) in a Boyden chamber culture system. An anti-ErbB antibody (Ab) and/or recombinant neuregulin 1 (Nrg1) were added to the relevant groups. The anti-ErbB Ab was added at the beginning of the coculture with BMDMs.

B. Representative images of immunocytochemical staining for p16. Primary cardiac fibroblasts were cocultured with or without H_2O_2. Nuclei were counterstained with 4□,6-diamidino-2-phenylindole (DAPI). Scale bars: 50 μm.

C. Quantitative reverse transcription-polymerase chain reaction analysis confirmed increases in expression of *SA-β-gal*, *p16*, and *p21* in cardiac fibroblasts cocultured with H_2O_2. $n = 4$ in each group. Data represent the mean ± SEM. $^{\#}P < 0.05$, $^{\#\#}P < 0.01$, $^{\#\#\#}P < 0.005$ versus normal cardiac fibroblasts (control); two-tailed, unpaired Student's *t*-test.

Expanded View Figure 4. ***Bone marrow-derived macrophages cocultured with H_2O_2-treated cardiac fibroblasts exhibit an M2-like macrophage phenotype.***

A. Representative images of immunocytochemical staining for CD68, CD14, F4/80, CD4, CD8, and CD31 in bone marrow-derived macrophages (BMDMs). Nuclei were counterstained with 4□,6-diamidino-2-phenylindole (DAPI). Scale bars: 50 μm.

B. Quantitative reverse transcription-polymerase chain reaction analysis confirmed increases in expression of pan-macrophage marker genes (*F4/80* and *CD11b*) and M2-like macrophage marker genes (*CD206*, *Arg1*, and *Fizz1*) in BMDMs cocultured with H_2O_2-induced senescent fibroblasts. Conversely, expression of M1 macrophage markers (*CD11c* and *MHC-II*) was decreased. $n = 4$ in each group. Data represent the mean ± SEM. $^{\#}P < 0.05$, $^{\#\#}P < 0.01$, $^{\#\#\#}P < 0.005$ versus BMDMs before coculture (control); two-tailed, unpaired Student's *t*-test.

Expanded View Figure 5. ***Nrg1 expression upregulates in bone marrow-derived macrophages, while cultured fibroblasts express Nrg1 receptors.***

A. Quantitative reverse transcription-polymerase chain reaction (qRT-PCR) analysis confirmed an increase in expression of *Nrg1* in bone marrow-derived macrophages (BMDMs) cocultured with hydrogen peroxide (H_2O_2)-induced senescent fibroblasts (H_2O_2) compared with BMDMs cocultured with normal fibroblasts (control). $n = 4$ in each group.

B. qRT-PCR analysis confirmed increases in expression of *ErbB2* and *ErbB4* in fibroblasts cocultured with H_2O_2 (H_2O_2) compared with normal fibroblasts (control). $n = 4$ in each group. Data represent the mean ± SEM. $^{\#}P < 0.05$, $^{\#\#}P < 0.01$, $^{\#\#\#}P < 0.005$ versus control; two-tailed, unpaired Student's *t*-test.

C. Double immunofluorescence staining showed that H_2O_2 enhanced expression of both ErbB2 and ErbB4 receptors. Nuclei were counterstained with DAPI. Scale bars: 10 μm.

Expanded View Figure 6. ***Expression of fibroblast activation-associated gene Spp1 increases in BMDMs.***

A and B. Quantitative reverse transcription-polymerase chain reaction analysis confirmed that expression of a fibroblast activation-associated gene (osteopontin [*Opn*]) (A) was increased in bone marrow-derived macrophages (BMDMs) cocultured with hydrogen peroxide (H_2O_2)-induced senescent fibroblasts. Conversely, the expression of other known fibroblast activation-associated genes (transforming growth factor-beta [*Tgfb*] and platelet-derived growth factor subunit A [Pdgfa]) (B) did not increase. $n = 4$ in each group. Data represent the mean ± SEM. $^{\#}P < 0.05$, $^{\#\#}P < 0.01$, $^{\#\#\#}P < 0.005$ versus BMDMs before coculture (control); two-tailed, unpaired Student's *t*-test.

Expanded View Figure 7. ***Trastuzumab does not affect apoptosis, senescence, inflammation, or fibroblast activation in the intact heart.***

A–D. Quantitative reverse transcription-polymerase chain reaction analysis showed no changes in mRNA expression levels of (A) an apoptosis-associated gene (*Casp3*), (B) senescence-associated genes (*SA-β-gal*, *p53*, *p21*, and *p16*), (C) senescence-associated secretory phenotype-associated genes (*CCL3*, *IL-6*, and *TNF*), or (D) a fibroblast activation-associated gene (*αSMA*) and fibrosis-associated genes (*Col1a1* and *Col3a1*) in mice after intraperitoneal trastuzumab injection compared with controls. $n = 4$ in each group.

Expanded View Figure 8. ***Trastuzumab does not affect the survival rate or body weight after MI.***

A. Trastuzumab was injected on the fourth, fifth, and sixth day after induction of myocardial infarction (MI). Samples were collected on the seventh, 12th, and 28th day after induction of MI.

B and C. Intraperitoneal trastuzumab injection did not affect the survival ratio or (C) change in body weight of MI mice. $n = 12$ in each group.

Expanded View Figure 9. ***In vivo inhibition of Nrg1 signaling promotes apoptosis and senescence of cardiac fibroblasts even in the remote area.***

A–C. Quantitative reverse transcription-polymerase chain reaction analysis showed post-myocardial infarction (MI) upregulation of (A) an apoptosis-associated gene (*Casp3*) and (B and C) senescence-associated genes (*SA-β-gal* and *p53*) in mice after intraperitoneal trastuzumab injection compared with controls. $n = 4$ in each group.

D. Double immunofluorescence staining of Thy1 and cleaved caspase 3 (CC-3) demonstrated that the ratio of apoptotic cardiac fibroblasts in the infarct area was increased in mice after intraperitoneal trastuzumab injection compared with controls at post-myocardial infarction (MI) days 7, 14, and 28. Arrow shows $Thy1^{+}CC\text{-}3^{+}$ cells. Scale bars: 100 μm. $n = 4$ in each group.

E. SA-β-gal staining demonstrated that senescence of cardiac cells in the remote area was significantly exacerbated in mice after intraperitoneal trastuzumab injection compared with controls at post-myocardial infarction (MI) days 14 and 28. Scale bars: 20 μm. $n = 4$ in each group. Data represent the mean ± SEM. $^{*}P < 0.05$, $^{**}P < 0.01$, $^{***}P < 0.005$ versus each group; $^{\#}P < 0.05$, $^{\#\#}P < 0.01$, $^{\#\#\#}P < 0.005$ versus the non-MI heart; one-way ANOVA.

Expanded View Figure 10. ***In vivo inhibition of Nrg1 signaling exacerbates myocardial inflammation and promotes accumulation of M2-like macrophages even in the remote area.***

A. Quantitative reverse transcription-polymerase chain reaction analysis showed post-myocardial infarction (MI) upregulation of senescence-associated secretory phenotype-associated genes (*CCl3* and *TNF*) in mice after intraperitoneal trastuzumab injection compared with controls. $n = 4$ in each group.

B. Immunohistochemistry showed that intraperitoneal injection of the anti-human epidermal growth factor receptor type 2 (HER2) monoclonal antibody trastuzumab significantly accelerated accumulation of $CD206^{+}$ M2-like macrophages in the remote area with a post-myocardial infarction (MI) peak on day 14. Scale bars: 100 μm. n=4 in each group. Data represent the mean ±

SEM. *$P < 0.05$, **$P < 0.01$, ***$P < 0.005$ versus each group; $^{\#}P < 0.05$, $^{\#\#}P < 0.01$, $^{\#\#\#}P < 0.005$ versus the non-MI heart; one-way ANOVA.

Expanded View Figure 11. ***In vivo inhibition of Nrg1 signaling activates cardiac fibroblasts even in the remote area.***

A. Double immunofluorescence staining of Thy1 and αSMA showed increases in accumulation and activation of cardiac fibroblasts in the remote area of the trastuzumab (HER2) group compared with the control group. Scale bars: 100 μm. $n = 4$ in each group.

B. Quantitative reverse transcription-polymerase chain reaction analysis showed post-MI upregulation of fibrosis-associated genes (*Col1a1* and *Col3a1*) in mice after intraperitoneal trastuzumab injection compared with controls. $n = 4$ in each group. Data represent the mean ± SEM. *$P < 0.05$, **$P < 0.01$, ***$P < 0.005$ versus each group; $^{\#}P < 0.05$ $^{\#\#}P < 0.01$, $^{\#\#\#}P < 0.005$ versus the non-MI heart; one-way ANOVA.

Expanded View Figure 12. ***In vivo inhibition of Nrg1 signaling exacerbates fibrosis even in the remote area.***

Masson trichrome staining showed that intraperitoneal trastuzumab injection significantly increased collagen fibrils in the remote area. Scale bars: 100 μm. $n = 4$ in each group. Data represent the mean ± SEM. *$P < 0.05$, **$P < 0.01$, ***$P < 0.005$ versus each group; $^{\#}P < 0.05$ $^{\#\#}P < 0.01$, $^{\#\#\#}P < 0.005$ versus the non-MI heart; one-way ANOVA.

Figure 1.

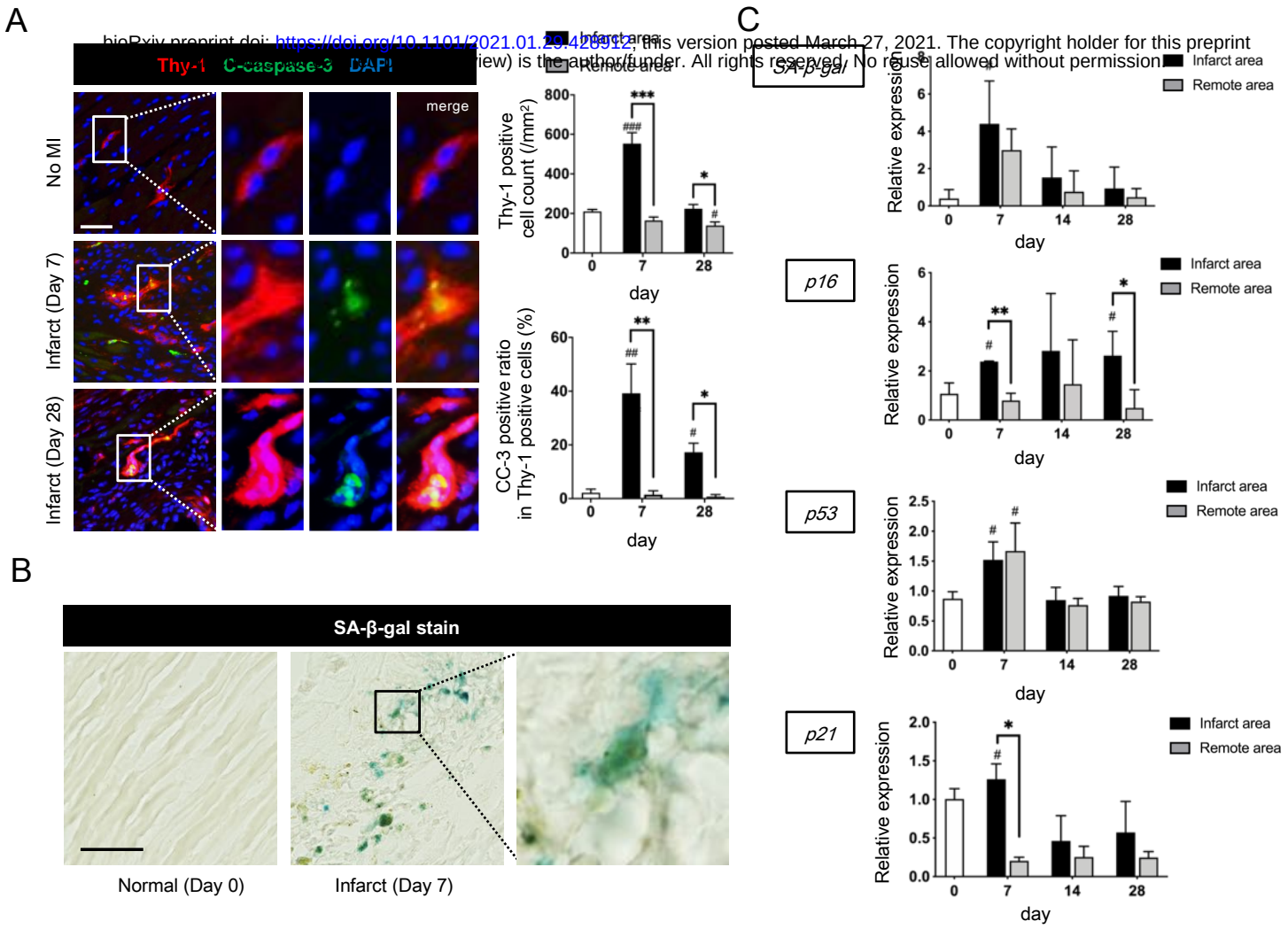

Figure 2.

A

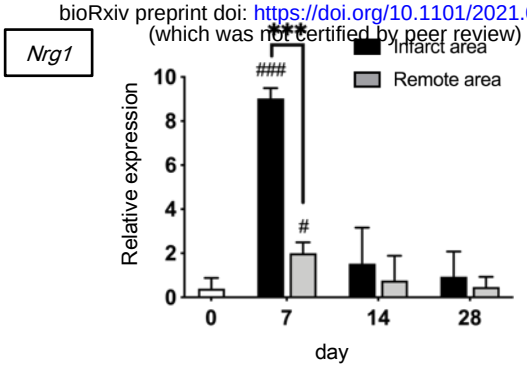

B

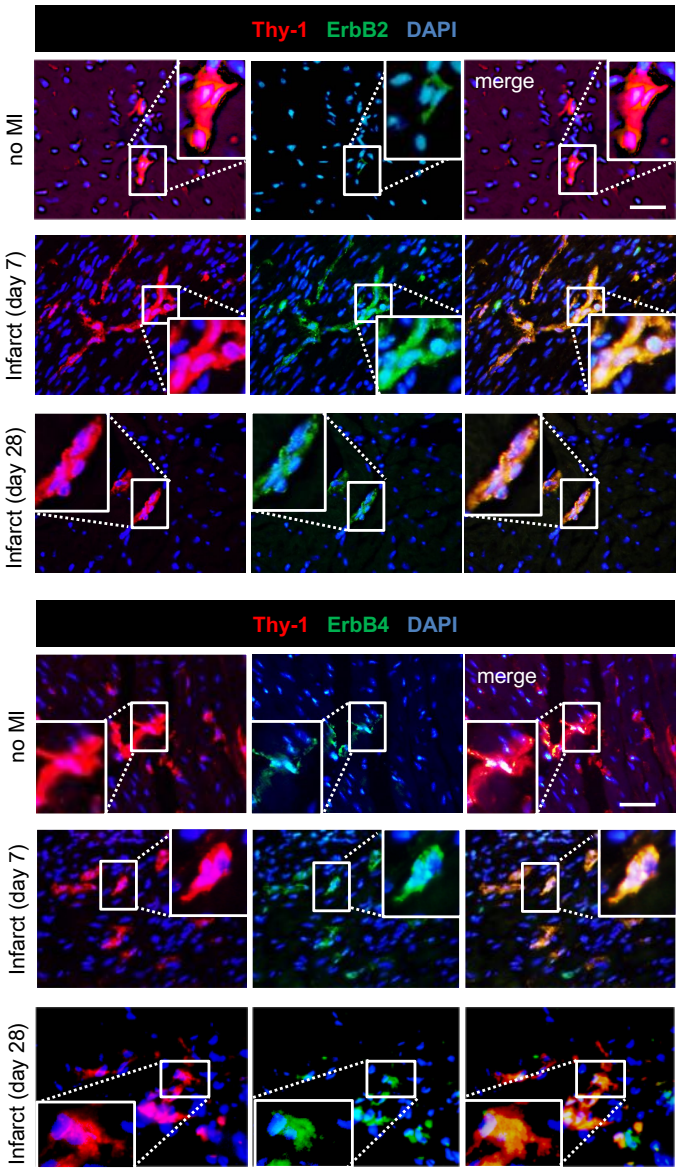

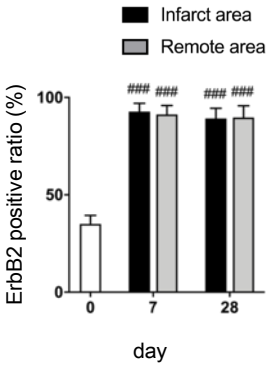

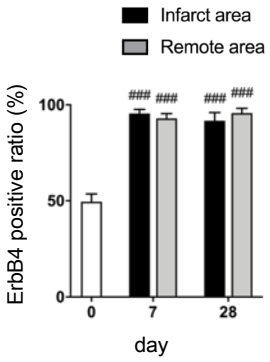

Figure 3.

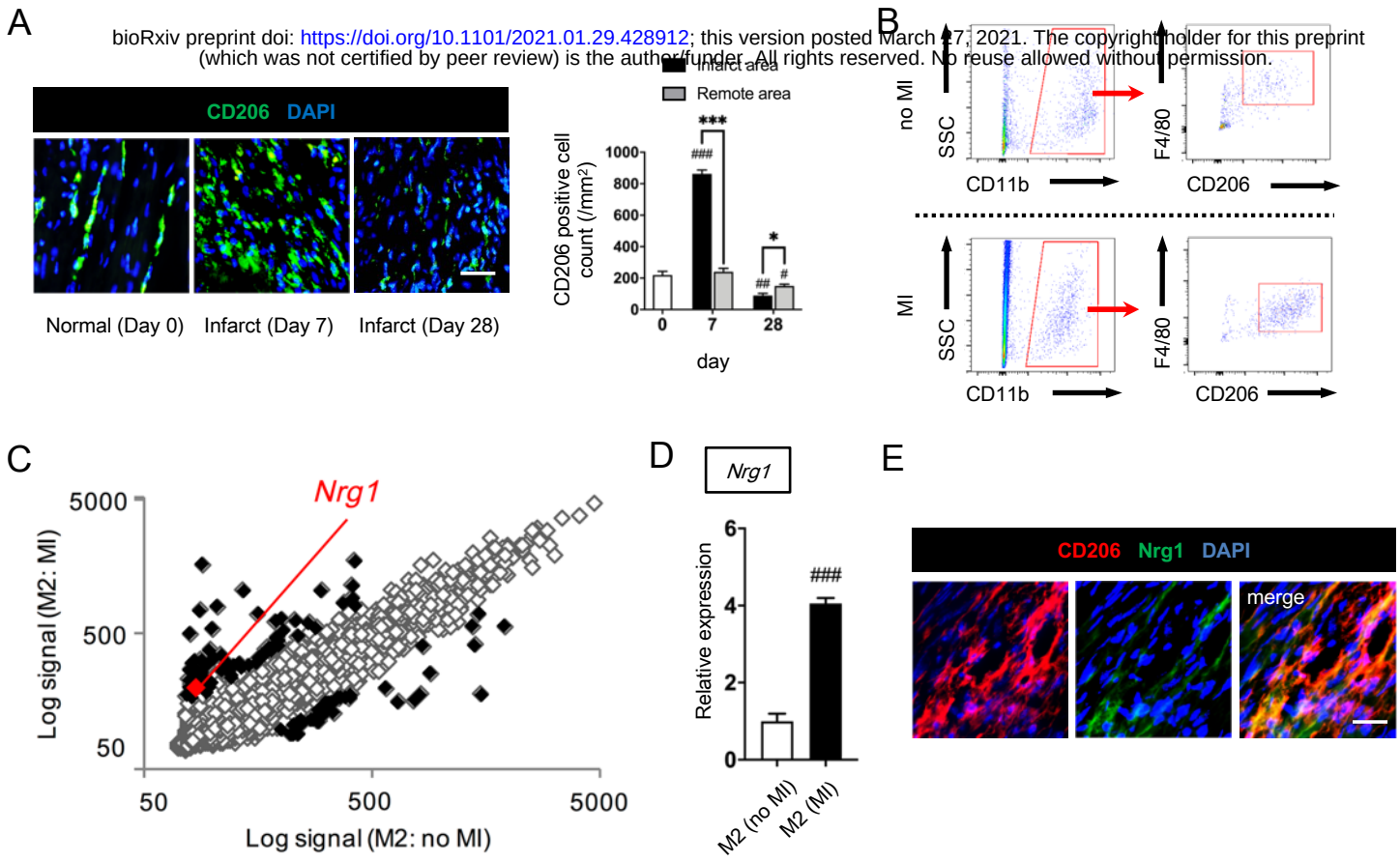

Figure 4.

A

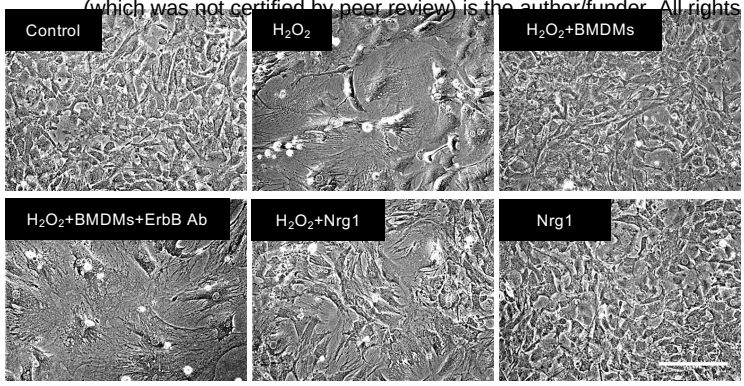

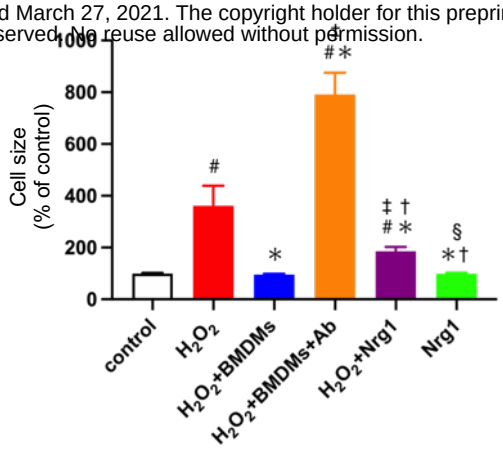

B

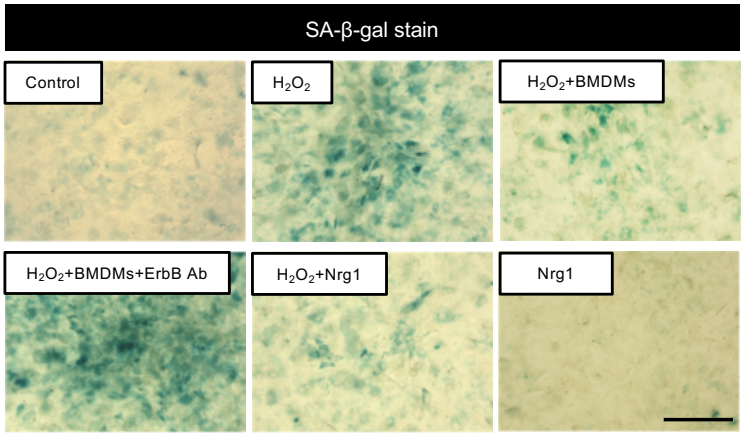

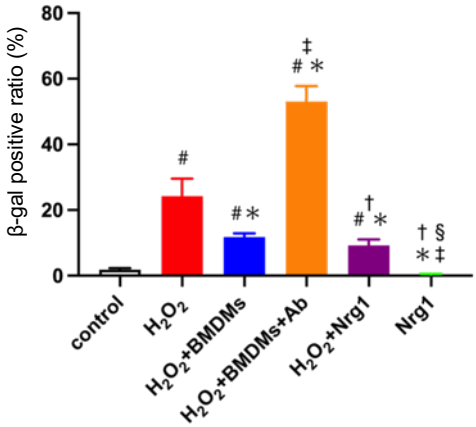

C

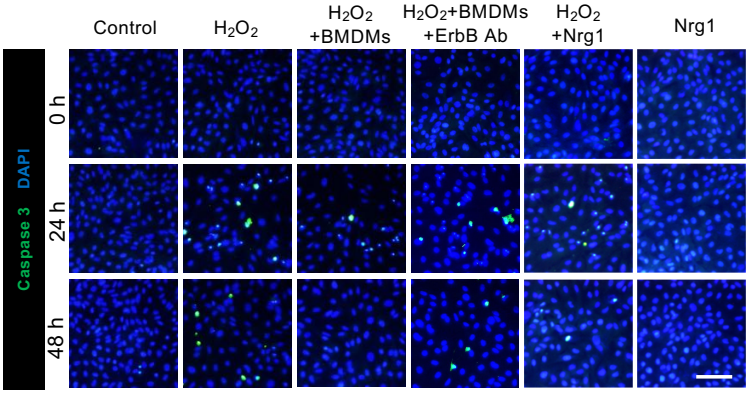

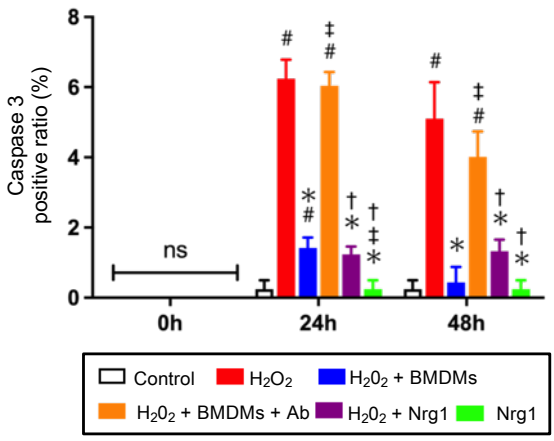

D

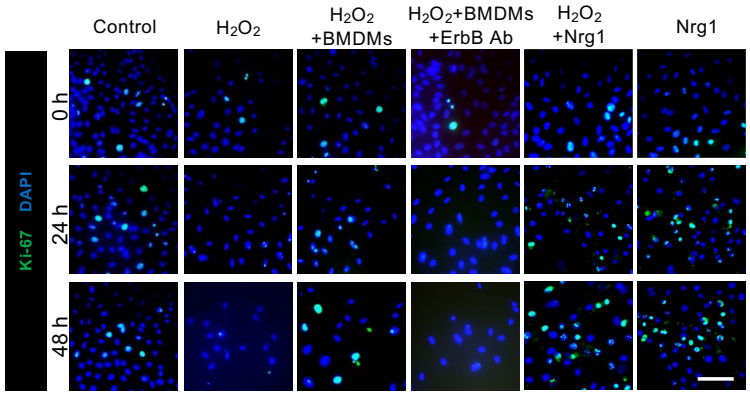

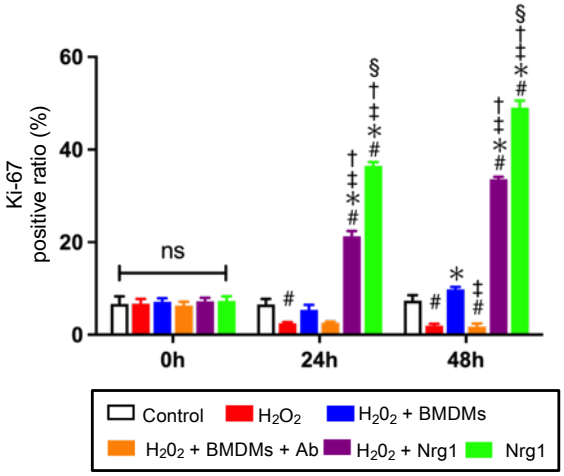

Figure 5.

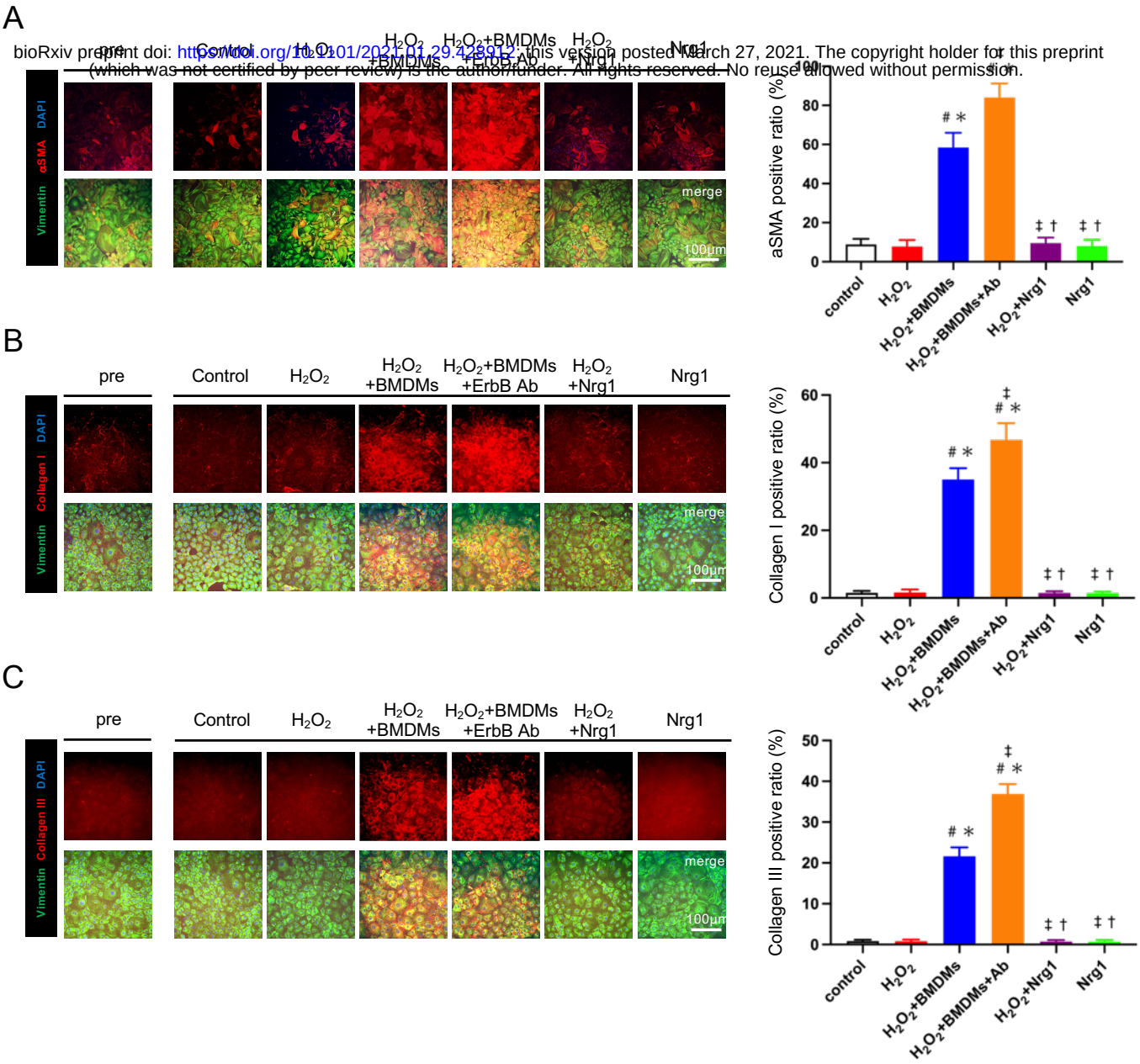

Figure 6.

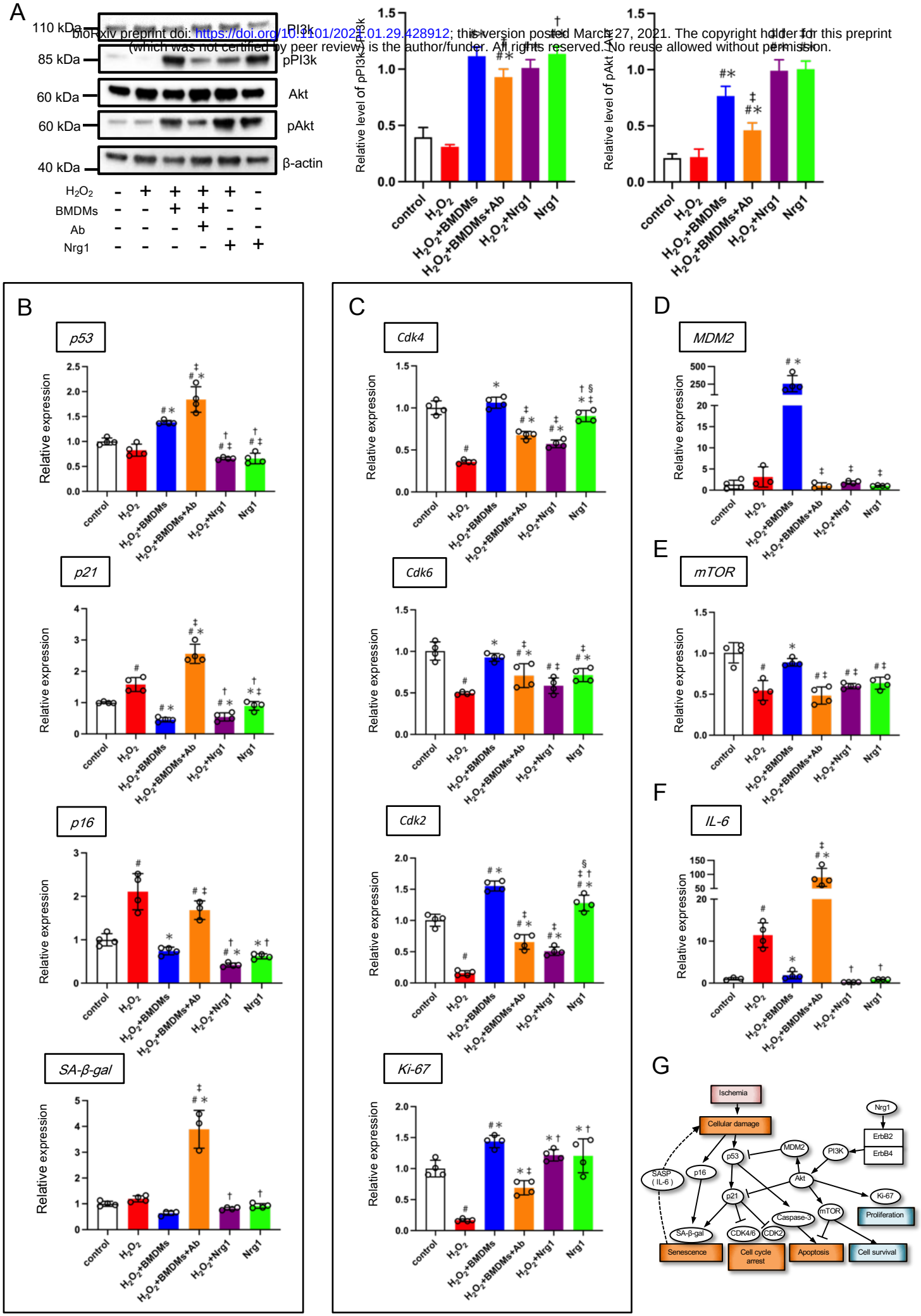

Figure 7.

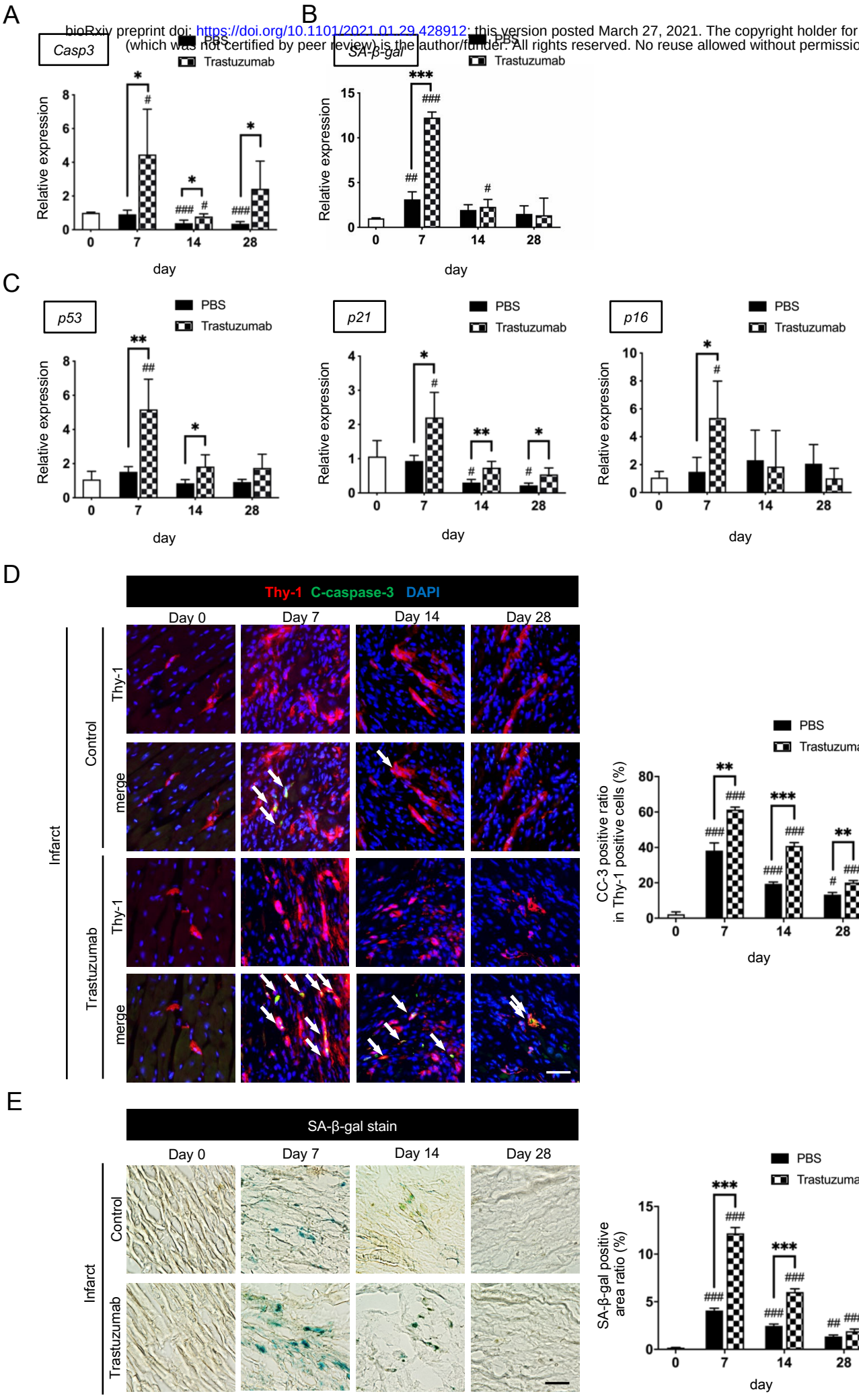

Figure 8.

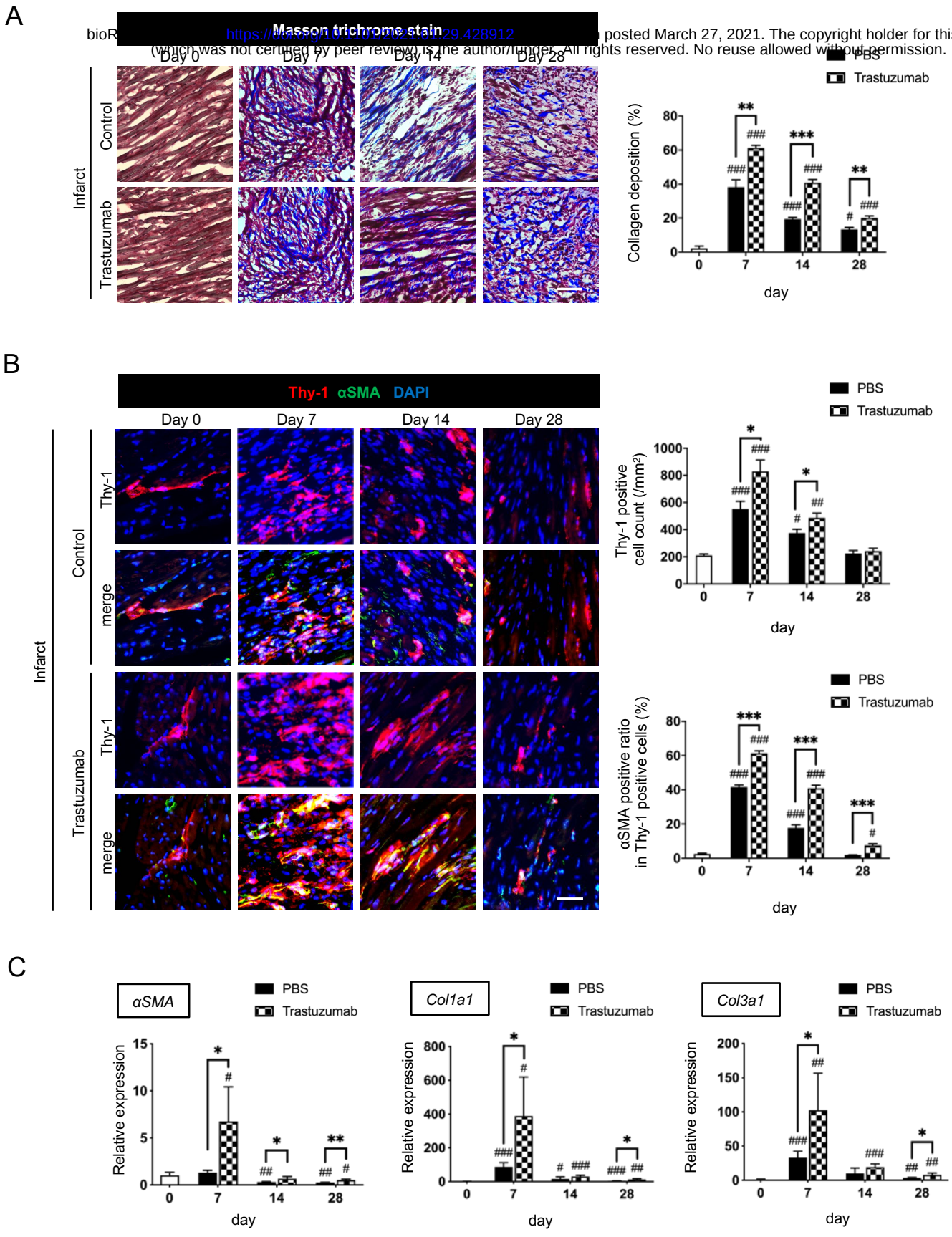

Figure 9.

A

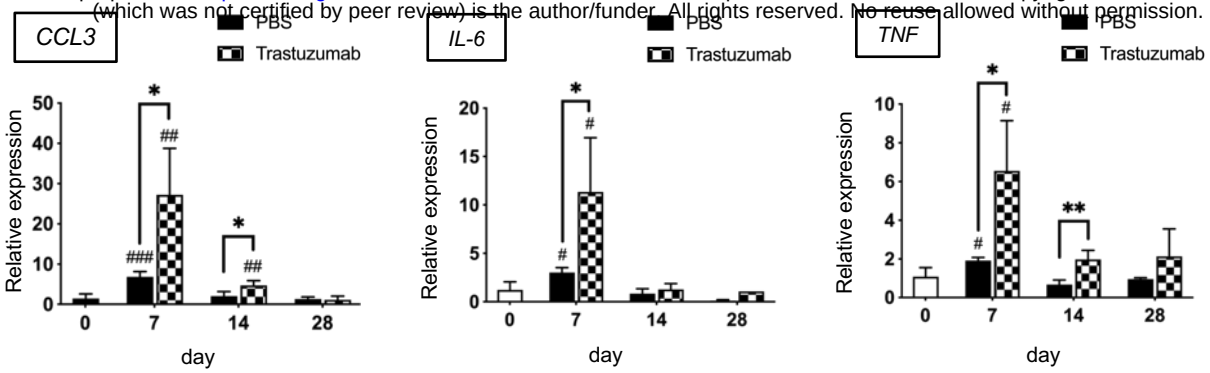

B

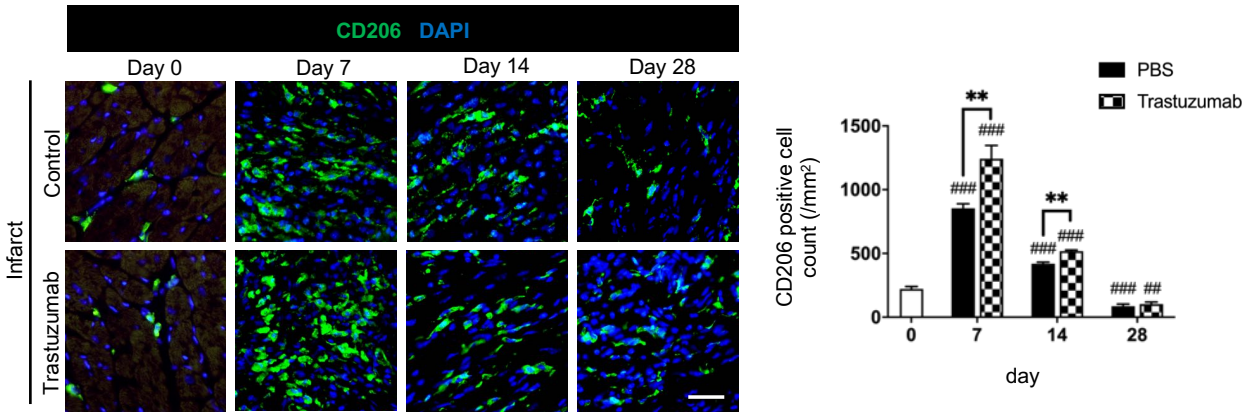

Figure 10.

A